2018-03-08

Vibrational Profiling of Brain Cells and Tumours using Atomic Force Microscopy

Nelson, Sultan

UNIVERSITY OF CALGARY

Vibrational Profiling of Brain Cells and Tumours using Atomic Force Microscopy

by

Sultan Nelson

A THESIS

SUBMITTED TO THE FACULTY OF GRADUATE STUDIES

IN PARTIAL FULFILMENT OF THE REQUIREMENTS FOR THE

DEGREE OF DOCTOR OF PHILOSOPHY

GRADUATE PROGRAM IN CARDIOVASCULAR AND RESPIRATORY SCIENCES

CALGARY, ALBERTA

March, 2018

Abstract

Nanoscopic mechanical vibration is observed as a periodic plasma-membrane fluctuation in living cells. The study of this physiological phenomenon is an emerging field of research. All prior experimental work has been limited to single cell study, including erythrocytes (1,2), leukocytes (3), and cardiomyocytes (4)**.** Moreover, the intensity of fluctuation has been shown to be indicative of cells' overall metabolic activity (5,6). The fluctuation can be modulated using pharmacological blockers (7,8), thus excluding stochastic Brownian motion as the sole explanation. Given our main interest in the potential clinical application of this phenomenon for qualitative and efficient brain tumor identification, we examined vibration waves emanating from cultured cells, and tissues harvested from the brains of newborn rats, as well as from brain tumors and neocortex specimens.

In this research project, we first developed a novel atomic force microscope-based (AFM-based) mechanical vibration detection method and a custom-written MATLAB vibration signal analysis algorithm. The AFM system used in this report utilized sensitive cantilevers (probes) to enhance the signal-to-noise ratio, and to improve overall performance. The method was also designed to detect cellular vibration without direct physical contact between the sample and the cantilever probe.

Using this unique method, we recorded vibrations emitted from newborn rat hippocampus and cerebellum samples; these brain regions showed distinct vibration profiles. The effect of pharmacological agents on the tissue samples examined suggested synaptic activity is the major contributor to the subtle vibrations observed. For assessment of potential clinical applications of the method, we examined human surgical brain biopsy samples. Malignant astrocytoma tissue

samples vibrated with markedly different frequency peaks and amplitude, compared to tissue from meningioma or normal lateral temporal cortex, thus providing a quantifiable measurement to accurately distinguish the three types of tissues. Lastly, we developed a method to convert cellular oscillation signals into sound within the frequency range of normal human hearing to provide medical specialists with a way to differentiate tumors from healthy brain tissue without the need for extensive, complex vibration, spectral analysis training.

Evidence attested through this project has shown that vibrational profiling of cells and tissues can be adopted for simultaneous mapping of neuronal and metabolic activity in the brain. Further, the results of this research may have translational clinical implications as a prompt diagnostic technique, which may aid clinicians in discerning between healthy and cancerous tissues in real-time.

Acknowledgements

This work would not have been possible without the dedicated support from the following people:

I would like to express my sincere gratitude to my immediate supervisor, Dr. Matthias Amrein, and to my supervisory committee, Dr. Garnette Sutherland and Dr. Francis Green for their support, guidance and encouragement throughout this novel and visionary research project.

The contents of this thesis are published in the journal *Theranostics*. (Nelson, Sultan L., et al. "Vibrational Profiling of Brain Tumors and Cells." *Theranostics* 7.9 (2017): 2417.) I would like to thank the Theranostics Editorial and Publishing team for providing me with permission to reuse and include its materials in this publication.

I would also like to thank the Project NeuroArm group, including Dr. Dustin Proctor, Dr. Ahmad Ghasemloonia, Dr. Sanju Lama, and Dr. Kourosh Zereinia for their expert advice and collaboration in this multi-disciplinary project. I thank the Dr. Michael Colicos Lab, in particular, Dr. Stephanie Stotz for providing live hippocampal and cerebellar neuron-glia co-cultures; Dr. Tak Fung for statistical consultation; Dr. Gregor Kuntze from the Human Performance Lab for input in MATLAB data filtering and analysis; Dr. Wee Yong and Dr. Sasobhan Sarkar for providing cancer cell lines; and Walter Hader for LTC specimens. Special thanks to Dr. Ali Tarokh for the constructive advice in the thesis preparation.

Many thanks to my dear friends – Dr. Mustafa Al-Saidy, Dr. Yahya Kinyogo, Daniella Urrego, & Salim Ghandorah for your on-going encouragement.

Dedication

This dissertation is gratefully dedicated to my beautiful wife Taralyn Nelson and son Reign Nelson. Thank you for your love, patience, and support.

I also would like to dedicate this work to all my family members both in Africa and here in Canada, who instilled the values of education and to persevere though life challenges .

Table of Contents

List of figures and illustrations

List of tables

Abbreviations

AFM = Atomic Force Microscope

AU = Arbitrary Unit

BT048= Slow growing brain tumor initiating cell line

EGF= Epidermal growth factor

EBS = Extracellular bath solution

FGF = Fibroblast growth factor

FFT = Fast Fourier Transform

GBM = Glioblastoma Multiforme

HFA= Human fetal astrocyte

LTC = Lateral temporal cortex

MR = Magnetic resonance

OCR = Oxygen consumption rate

OT = Optical Trap

PFA= Paraformaldehyde

PET = Positron emission tomography

SEM = Standard error of mean

TTX= Tetrodotoxin

RMS = Root Mean Square

U178 = Fast growing (aggressive) glioma cell line

Chapter One: **General Introduction**

1.1 Motivation

Total resection is the primary goal for preventing the recurrence and malignant transformation of many brain tumors. However, optimal surgical resection may be limited by the challenge of differentiating normal, healthy brain tissue from that infiltrated by tumor cells (9,10). As a result, resection is invariably incomplete, and for glioma, tumor recurrence inevitable. This is further complicated by the location of the tumor and its proximity to eloquent structures (11). While techniques of tissue interrogation for resolving the brain-tumor interface are evolving -- e.g. Raman spectroscopy (12), positron emission tomography (PET) (13), MR spectroscopy (14) and 5-Ala fluorescence guided surgery (15) -- they are not without significant challenges and limitations (e.g. local properties or low sensitivity). Furthermore, no existing technology, nor those under development, can characterize definitively, the tumor type, or its malignancy grade. A precise diagnosis still relies on a qualitative, post-surgical histopathological and genetic characterization. This precludes any immediate action during surgery, and delays the use of other adjuvant treatments.

Maximizing brain tumor resection requires the development of a novel tissue interrogator that can, in real time, probe the metabolic profile and tissue type with accuracy and sensitivity. In this study, we introduced a novel and robust AFM-based method to detect nanoscale vibrational outputs from live cells, brain tissues, and tumors. We have shown this unique method can differentiate live specimens of high-grade astrocytoma, meningioma, and healthy neocortical tissue through vibrational spectrum fingerprinting and by analyzing the intensity of fluctuation. An advancement to existing technologies, this new method provides diagnostic information concurrently, on both tumor type and metabolic activity. We also constructed acoustic signatures

of astrocytoma, meningioma, and neocortical tissues from vibration recordings that may allow neurosurgeons to interrogate the brain-tumor interface by sound, while performing surgery.

1.2 Detection of nanomechanical vibration emitted from cells

Nanoscopic cell surface mechanical vibration is observed as a periodic plasma-membrane fluctuation in living cells (5,6,8,16-19). The study of this subtle, physiological phenomenon is an emerging field of research. All previous experimental work has been limited to the study of single cells. For specific cells, including erythrocytes, leukocytes, cardiomyocytes and neuroblasts, cellular vibration with frequency peaks in the range of 0.2 to 30 Hz have been reported (4), suggesting that these nanomechanical oscillations are a common feature of living cells.

Previous studies, using the cantilever of an AFM in contact mode, have shown the mechanical oscillation of single prokaryotic and eukaryotic cells (5-8,18). For example, Pelling et al 2004, using the contact-AFM method, reported dominant frequency peaks at 1-1.6 kHz for Saccharomyces cerevisiae (6). One of the technical challenges in translating vibration recordings to clinical application has been how to improve the signal-to-noise ratio of AFM-based systems. Further, capturing nanoscopic oscillations from mammalian cells which are, at least an order of magnitude lower in amplitude and power than yeast cells, has remained a significant challenge.

Improvements in the manufacture of ultra-sensitive cantilevers have very recently provided the capacity to accurately measure fluctuations in soft biological samples. For example, since the original Pelling et al 2004 observation there has been a significant advance in cantilever tip production such as Silicon Nitride (BL-RC-150VB, Olympus) with nominal spring stiffness 0.002 – 0.016 N/m, while Pelling and colleagues used .06 N/m. This is at least a 30-fold increase in the

sensitivity. Fluctuations have now been recorded for cultured mammalian cells adherent to a cantilever (5,8). While these latest reports demonstrate the ability of an AFM to detect vibration from mammalian cells, it is unclear that they have the sensitivity to extract spectral contents from the acquired signals. It is also important to note the vibration of more complex biological systems, such as tissue, has not been examined previously.

1.3 Clinical correlations of cell vibration

The physiological mechanisms that generate, drive and coordinate cell surface vibration are not well understood. Therefore, understanding the environmental, physiological, and pathological factors that affect the characteristics of cell vibration need extensive investigation. Some studies report promising results determining the effect of pathological conditions on cell vibration. For example, the ability of hematogenic cells to pass unhindered through vascular capillaries is correlated to membrane fluctuation (20). Further, changes in cellular vibration have been reported in patients with lymphoma and severe diabetes, as compared to healthy controls (3,21).

The viscoelastic properties of cells, such as membrane stiffness, are also associated with the metastatic potentials of lymphoma (22) and carcinoma cells (23). These structural properties of cells are closely interlinked with cytoskeletal proteins that govern membrane elasticity and compliance, which in turn, may alter the characteristics of cell membrane vibrations (24). Specifically, the chemotherapeutic agent paclitaxel has been shown to significantly reduce the intensity of vibration of cancer cells (8). This result suggests that the cytoskeleton and the dynamic instability of microtubules are major factors in generating the magnitude of cell vibrations (8). A similar reduction in amplitude has been reported when red blood cells' (RBC's) membrane

skeleton was denatured (25). A higher intensity of oscillations was seen with metastatic lymphoma cells compared to non-metastatic lymphoma (26). Treating metastatic cancer cells with chemotherapeutic agents that disrupt the microfilaments have been shown to inhibit the ability of cancer cells to metastasize (27). These results suggest that specific aspects of cell vibration are correlated to the metabolic state of cells, which can be detected and monitored (28).

1.4 Overview of Glioma

The word 'glioma' is an umbrella term used for all tumors that are thought to be of glial cell origin[1]. Neuroglia are subtype of glia in the central nervous system (CNS), which are derived from ectoderm during embryogenesis (92). These include astrocytes, oligodendrocytes and ependymal cells. These cells play key roles in facilitating efficient and proper functions of neurons (89). Relatively rare environmental and genetic syndromes have been shown to alter the normal functions of glia cells to cause glioma. For example, exposure to therapeutic high doses of ionizing radiation are predominantly associated with the cause of glioma (88). A few genetic syndromes that are caused by rare inherited mutations have also been associated with increased risk of gliomas (88). As a proof of concept and in order to limit the scope of this project, we will focus on this astrocytic derived brain tumors.

1.5 Classification of Glioma

Current definitive diagnosis of glioma still relies on a post-surgical histopathological and genetic characterization (89). According to the World Health Organization (WHO) standard classification, astrocytomas are classified as grades I, II [astrocytoma], III [anaplastic astrocytoma], and IV [glioblastoma or glioblastomamultiforme (GBM)] (88), which is based on histological and predominantly morphological changes observed under microscope (93). This

grading system is facilitates communication among clinicians and scientists, and used to plan treatment and predict outcome (93). For instance, the grade of a tumor is used to indicate the aggressiveness or malignancy of a tumor. Studies suggest that low grade (I & II) is often indicative of slowly growing tumor with relatively normal morphological appearance (93). While high grade tumors (III & IV) are by definition malignant and are characterized by bizarre appearance and rapid growth[6]. These tumors are also form new blood vessels to meet the demand for more nutrients during fast growth (93).

1.6 Treatment and Intervention of Glioma

Surgical intervention is the gold standard and often the first step to treat anaplastic astrocytoma and glioblastoma aiming at obtaining tumor sample for diagnosis confirmation, treatment plan, relieve pressure and safely remove as much tumor as possible (93). Subsequently, radiation and chemotherapy could be used for further treatments[6]. However, tumor grade, size and location are taken into consideration to determine treatment plans and prognosis of gliomas (93).

The most important goal of neurosurgeons during surgical procedure is that maximizing resection of brain tumor to prevent recurrence while preserving function, which requires high precision mapping of the tumor brain interface. We believe that vibrational profiling using Atomic Force Microscope (AFM) and Optical Tweezers might be powerful tools to aid such diagnosis and management of cancer.

1.7 Objectives of the current project

We custom-developed a novel atomic force microscope (AFM) based nanomechanical force detector and signal analysis algorithm to study vibrations emanating from single cells and complex tissue samples. The AFM system used high-sensitivity cantilevers (probes) to enhance

the signal-to-noise ratio, and to improve overall performance. Furthermore, the method detected cellular vibration without direct physical contact between the sample and the cantilever probe. The AFM experimental apparatus was improved further with the inclusion of a spectrum analyzer that allowed real-time feedback of signals, which was used for the rapid characterization of biological samples.

In Chapter 2, we assessed the capability of the proposed method using cultured cells and tissues harvested from the brains of newborn rats. The results from this ex-vivo animal model study suggested that vibrational profiling of cells and tissues can be used to simultaneously study neuronal activity, and the overall metabolic status of the brain. This enabled us to distinguish brain regions by the different metabolic activity of the hippocampus and the cerebellum. Furthermore, our studies examining the effects of pharmacological agents on brain tissue showed that synaptic activity is the source of the frequency profile and a major contributor to the intensity of cell fluctuation.

Building on the promising results in the animal model studies, Chapter 3 deals with the clinical assessment of the newly proposed method to discern between healthy and cancerous tissues. In this section, we show intensity of fluctuation, measured in root mean square (RMS), is linked to the aggressiveness (energy consumption) of the type of cancer. We demonstrate this critical finding using cultured human astrocytes (HFA), slow-growing (BT048), and fast-growing (U178) cancer cells. Single cell examination of these three cell types using optical tweezes resolved distinct frequency peaks up to 50KHz.

Given the marked differences in cultured neuronal cells, we applied these techniques to human brain tumor biopsies, including malignant astrocytoma, meningioma and lateral temporal

cortex, adjacent to the exciting focus. We used tissue from patients with epilepsy as a control. Human malignant astrocytoma vibrated with a markedly different frequency profile and amplitude, compared to tissue from meningioma or lateral temporal cortex, thus providing a quantifiable measurement to accurately distinguish the three types of tissue.

In this thesis, we also describe a method to convert oscillation signals into sound within the frequency range of normal human hearing. This would provide medical specialists with a medium to differentiate tumors from healthy brain tissue without the need for complex signal analysis.

Chapter Two: **Assessing AFM contact free mode capability to detect vibration in mammalian cells**

2.1 Introduction

The AFM is an important device for studying the mechanical and structural properties of cells including membrane stiffness (29,30), high-resolution surface imaging (31,32), molecular adhesion forces of cellular components (33) and molecular-scale pharmacological interactions (34). The AFM is also capable of detecting cellular vibration from individual cells in contact-mode with the sample (5,6,8). Capturing nanoscopic oscillations from mammalian cells which are at least an order of magnitude lower in amplitude and power than yeast cells, has remained a significant challenge to the field. However, recent improvements in manufacturing more sensitive cantilevers have made it possible to measure fluctuations in biological samples. Specifically, it is now possible to measure fluctuations in cultured mammalian cells adherent to a cantilever (5,8).

Even though it is possible to detect nanoscale oscillations from mammalian cells, detecting oscillations remains limited to recording fluctuations from a small region of interest. (i.e. The direct interface point between the cantilever tip and sample.) This is of concern as mechanical properties vary from point to point across the surface of a cell (33). Therefore, fluctuations recorded from classical contact-AFM techniques are unlikely to be representative of the whole cell. A contact-free AFM system might eliminate this problem and give a more accurate measure of a cell's fluctuations. In addition, it would allow the study of nanoscale fluctuations for complex systems, such as tissues.

The main objective of this chapter is to assess the capability of a contact-free AFM technique to detect cell and tissue vibration using cells and tissues from animal models. In this chapter, using the contact-free AFM technique, we show that cells and tissues of mammalian origin

vibrate with reproducible and distinct frequencies. We demonstrate this by distinguishing between two anatomically distinct regions of newborn rat brain by characterizing their amplitude and spectral patterns of vibration. We also show the effects of pharmacological agents on the vibrational signals, thereby providing information on the driving sources of the vibrations and allowing us to explore the potential of the AFM method as a real-time, drug testing platform. We hope the studies described in these chapters serve to lay the foundation for a novel method to study cell and tissue properties. We believe this will have both basic science and clinical relevance.

2.2 Methods and Materials

2.2.1 AFM Experimental design and data acquisition protocol

A customized JPK NanoWizard® II AFM linked to a spectrum analyzer (RSA3300A, Tectronix) recorded cell and tissue vibrations. The AFM experimental setup is schematically depicted in Figure 2.1. The setup was comprised of three parts: An inverted light microscope used for a visual inspection of samples, a cantilever (BL-RC-150VB, Olympus) used as a vibration sensor or detection probe, and a spectrum analyzer for real-time spectral analysis. In this case, the spectrum analyzer monitored the stability of the vibrational signal prior to recording, and established an appropriate sampling frequency based on Nyquist theorem. The AFM system and materials were housed in a custom-built incubation chamber that maintained a consistent temperature of 37°C. Likewise, a pump, designed in-house, maintained a 5% CO_2 environment. The pump was turned off and the AFM was placed on a large air-table during recording to exclude external sources of vibration. The feedback loop was also turned off after setting the cantilever distance, 15 µm above the surface of the dish and approximately 5 µm laterally displaced from tissue samples, to avoid noise signal leakage into the recordings. For further offline analysis, 30 seconds of force fluctuations were logged from brain cultured cells and tissues. For each given cell culture and tissue experiment, we recorded three 30-second segments of vibrational signals. For all protocols, independent experiments were performed on at least three separate biological preparations.

A

B

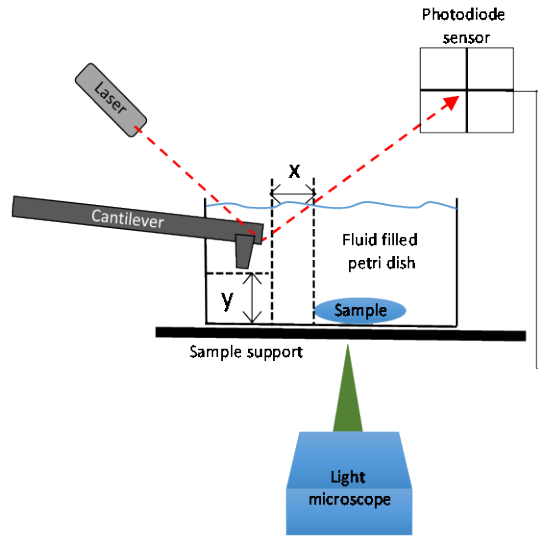

C

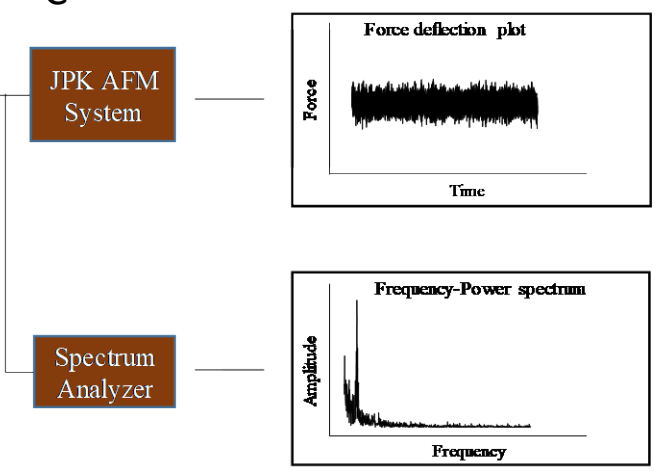

D

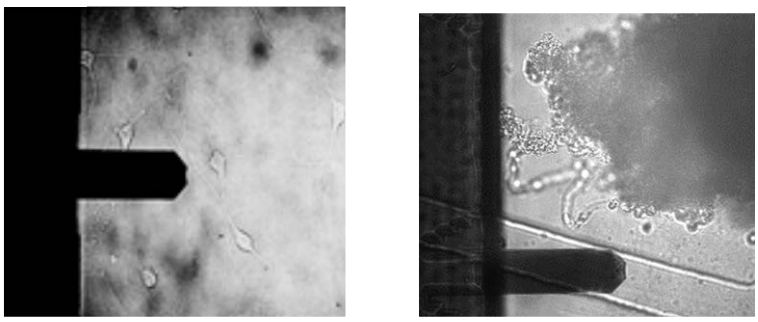

Cultured neurons

Neural tissue

Figure 2.1: AFM contact-free detection system to measure cell culture and tissue vibration. (A) Picture of AFM with the custom-built housing. (B) Schematic of contact-free AFM detection system to measure tissue vibration, and an example of light microscope images of the cantilever approaching the biological sample in the recording solution. The probe is placed ~15 µm from the bottom surface of the dish. A planar wave propagation emanating from the sample is depicted as lines. Note: the cantilever, sample and waves are not drawn to scale. (C) Laser deflecting off the cantilever tip is detected by a photodiode sensor and analyzed with the JPK AFM system and real-time spectrum analyzer to produce force deflection curves and frequency power spectrum plots respectively. (D) Representative hippocampal pyramidal neuron grown in culture, and a hippocampal tissue piece in recording solution are shown.

We calibrated systems as per manufacturing guidelines prior to conducting all experiments. (JPK user's manual.) Briefly, we determined the cantilever's spring constant and resonance frequencies. The nominal spring stiffness for cantilevers (BL-RC-150VB) of 0.002 – 0.016 N/m provided by the manufacturer (Olympus) was used to compare our experimentally derived spring constants that were determined for each experimental run. We also determined the spring constant for each cantilever by implementing analysis of thermal noise during calibration. JPK's AFM software enables users to calculate the resonance frequency of each cantilever in a liquid solution from the recorded thermal noise spectrum. The nominal resonance frequency of the cantilever was 7 – 21 kHz. The thermal resonance curve dominant frequency peak can be fitted to Lorentz function, which also allowed computation of the spring constant. The nominal resonance frequency of the cantilever was well above the frequency range of our interest in this study.

2.3.1 Pharmacological agents used as recording solutions

Resting state media or extracellular bath solution *(EBS):* 135 mM NaCl, 3 mM $CaCl_2$, 5 mM KCl, 2 mM $MgCl_2$, 10 mM glucose and 5 mM HEPES, pH 7.4, 315 mOsm

High-K^+ depolarization buffer*:* 115 mM NaCl, 3 mM $CaCl_2$, 30 mM KCl, 2 mM $MgCl_2$, 10 mM glucose and 5 mM HEPES, pH 7.4, 315 mOsm

Ca^{2+}-free High-K^+ buffer*:* 115 mM NaCl, 30 mM KCl, 2 mM $MgCl_2$, 10 mM glucose and 5 mM HEPES, 10 mM EGTA (ethylene glycol tetraacetic acid), pH 7.4, 315 mOsm

Tetrodotoxin (TTx) buffer*:* EBS + 1 µM TTx

Sodium azide buffer*:* EBS + 1 mM NaN_3

2.3.2 Hippocampal and cerebral culture cell preparation and recording

All experimental protocols were approved by the University of Calgary Conjoint Faculties Research Ethics Board (Protocol # AC17-0051). Dissociated hippocampal and cerebellar neuron and glial co-cultures were prepared from P0 Sprague–Dawley rat pups (Charles River, Wilmington). Culture dishes were treated overnight with poly-d-lysine (Sigma-Aldrich, St. Louis) (50 µg/ml working dilution). Dishes were then washed trice with PBS and incubated for three hours with mouse laminin (Sigma-Aldrich) at a final concentration of 10 µg/ml.

Animals were anesthetized on ice and sacrificed by decapitation. Brains were removed and placed into ice-cold dissection media. (Hank's balanced salt solution supplemented with 8.4 mM HEPES pH 7.2, adjusted to 310-320 mOsm with sorbitol.) Selected brain regions, hippocampi and cerebella, were dissected out and meninges removed.

For culture preparation, hippocampi and cerebella were incubated in enzymatic solution with 20 µl/ml of papain for cell dissociation. After 30 minutes, cells were washed three times in growth medium (BME (Invitrogen), supplemented with B27, penicillin, streptomycin and l-glutamine). Subsequently, cells were triturated using three decreasing calibers of trituration pipettes and plated at 0.25×106 (1-week cultures) 1×106 cells (2-week cultures) per dish in growth medium + 4% fetal bovine serum (Invitrogen). Cultures were maintained with 4% Fetal Bovine Serum (FBS) for the first week to aid establishment of the cultures; FBS were subsequently reduced to 1% to restrict growth of the astrocytes.

2.3.3 Hippocampal and cerebellar tissue preparation

For vibration studies at the tissue level, we used hippocampal and cerebellar tissues excised from newborn rat brains. For each experiment, we logged vibration signals using approximately 8×10^6 μm^3 pieces from each region of newborn rat brain, taking care to maintain consistent tissue dimensions. To maintain a resting state tissue, we incubated the tissue in EBS. The tissue samples were subsequently fixed with 4% PFA.

2.3.4 Protocols for deciphering biological properties of vibration

Five protocols were used to investigate the effect of pharmacological agents on tissue vibration. The five protocols were similar for both hippocampal and cerebellar tissues. We used similar AFM experimental setups for all protocols, as described in Methods and Materials 2.2.1. In the resting state, Protocol 1, vibration signals were recorded from tissues bathed in EBS medium only. In the second protocol, tissues were transferred into a high-K^+ buffer. In Protocols 3 & 4,

recordings were conducted in a Ca^{2+}-free high-K^{+} and TTx solutions respectively, to block neuronal activity. Finally, tissues were fixed in PFA for 48 hours prior to conducting Protocol 5.

2.3.5 Data analysis

All data acquisition and vibration signal analysis protocols were developed specifically for this project using MATLAB, a technical computing environment developed by MathWorks Inc (USA), These protocols were used for computation and data visualization. Details of the script used is presented in Appendix B. Note, the wavelet-based, signal high pass frequency filtering algorithm adopted in the custom script was completed with the permission of the Human Performance Lab, at the University of Calgary. Overview of the computational analysis is presented as a flow chart in Figure 2.3 followed by a brief description of the chart.

2.3.6 Statistical analysis:

One-way ANOVA was used to compare mean RMS amplitudes in cases where more than two data groups were present. N-values represent biological replicates carried out for each cell-line, primary culture or tissue preparation. For each biological replicate 3 technical replicates were performed. Tamhane post hoc analysis was used to determine statistical significance. Independent t-test were used to compare mean RMS amplitudes were differences between two groups were analyzed. Normal probability plots were used to check the normal distribution of the frequency peak clusters for brain tumor and lateral temporal cortex specimens.

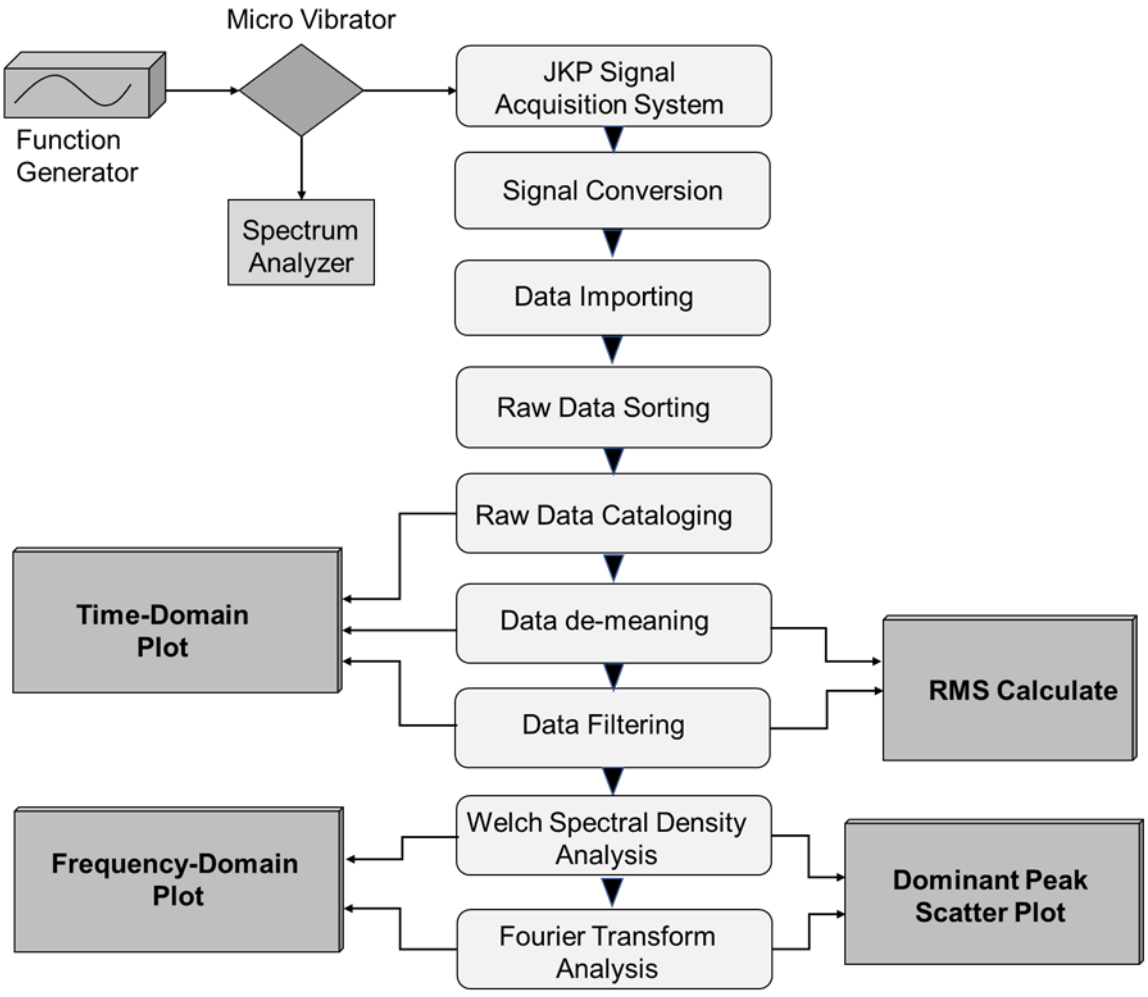

Figure 2.3: Flow chart for the computational analysis of vibration. A MATLAB algorithm was developed to automate the acquisition of the raw data, as well as for analysis, pattern extraction and interpretation

Recorded data was exported from JPK software as text (.txt) format and then converted to an excel (.xlsc) document prior to MATLAB data analysis. Then, the custom- written script sorted three repeats of force deflection columns for each experiment conducted with corresponding segmental times. The extracted force deflection signals were then plotted to reveal the time domain vibration patterns. To adjust for the cantilever tip drift that commonly occurs during recordings, signals were demeaned. By dividing the force deflection points by spring constants used, we were able to obtain the vertical deflection signals used to calculate Root Mean Square (RMS) amplitude in the time domain. The customized MATLAB program also computed Fast Fourier Transform (FFT) that converted the force deflection signals in the time domain to the frequency domain. For spectral analysis, a major frequency peak was defined as frequencies with amplitude 10 dB/Hz above the amplitude of their adjacent frequencies in Welch's power spectral density plots. The RMS results and frequency domain spectrums were plotted to compare the different groups.

2.3.7 Statistical analysis:

We used one-way Analysis of Variance (ANOVA) to compare mean RMS amplitudes in cases where more than two data groups were present. N-values represented biological replicates carried out for each cell-line, primary culture, or tissue preparation. For each biological replicate, we performed three technical replicates. Tamhane post hoc analysis determined the statistical

significance. We used independent t-tests to compare mean RMS amplitudes to analyze between two groups.

2.4 Results & Discussions

2.4.1 Baseline recording and identifying external sources of vibration

The main objective of this section was to determine and assess the presence of external sources of vibration in the setup of the experiment. External sources of vibration served as a control to compare subsequent tissue and cell vibrational measurements. Prior to conducting experiments, the system was calibrated as described in Methods and Materials 2.2. Spring stiffness of the cantilever was calculated and assigned a constant value "*K*" according to Hook's Law of spring constant. The cantilevers had an average constant "*K*" value of 0.0049 ± 0.0005 N/m, which was consistent with the cantilever stiffness recognized by the manufacturer. Soft cantilevers, such as the ones used in this study, have superior nano-scale force detection capability; however, they are susceptible to thermal fluctuations and drift (33). In order to assess and quantify this inherent physical property of the cantilevers, we determined internal baseline vibrations from extracellular bath solutions (EBS) containing no sample. A sample plot of thermal fluctuation is shown in Figure 2.4A. Note the effect of cantilever drift depicted as a noticeable downward slant, and the overall cantilever fluctuation in this time domain plot. Figure 2.4B shows the demeaned signal, where analytical processing is implemented to remove the average of the original recording, adjusting for the downward slant in Figure 2.2A. All vibration signals recorded underwent this adjustment process to realign, and therefore negate, cantilever drift. This processed signal was used to calculate all root mean square (RMS) amplitude computations.

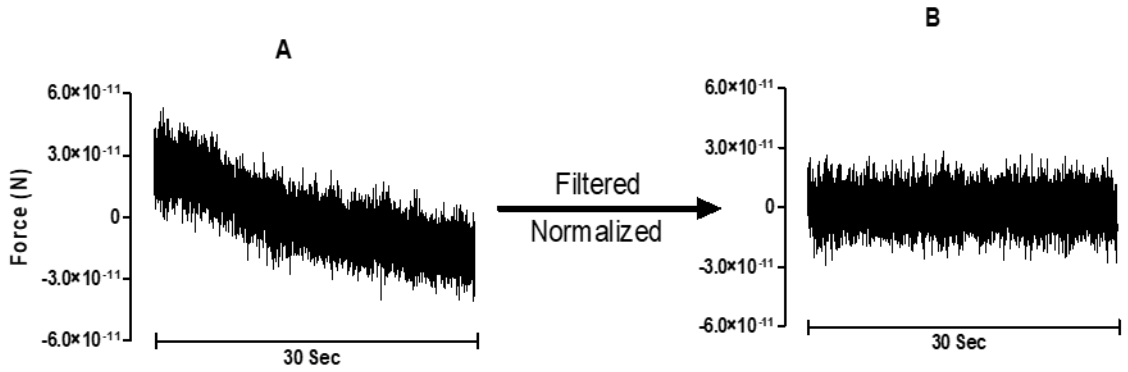

Figure 2.4: Sample force deflection curve of 30 seconds. Representative time domain recording of cantilever thermal fluctuation (A). Post processing of the signal, using wavelet based high-pass filtered with 1 Hz cut-off frequency and demeaned to correct for cantilever drift (B).

Frequency domain analyses of signals recorded from petri-dishes containing no samples also revealed normal noise spectra of the cantilevers used, plus some minor interference at 120 Hz and higher harmonics thereof. A representative frequency domain plot is shown in Figure 2.5. Therefore, the major frequency peaks observed were determined to be non-cell dependent peaks, and were eliminated in further cell and tissue spectral analyses. All these initial time and frequency domain findings were quantified as baseline RMS amplitude due to thermal fluctuations of the cantilever and control frequency peaks, and other system power interference.

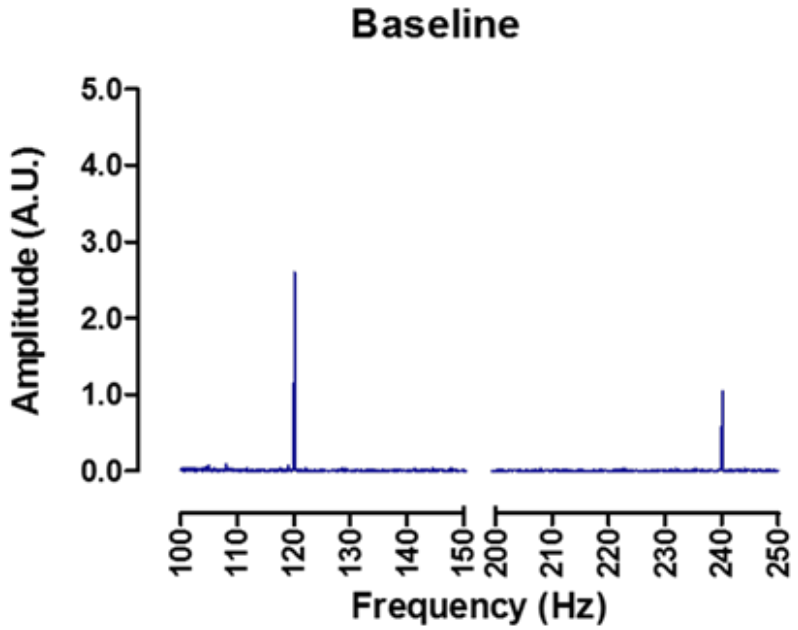

Figure 2.5: Frequency spectrum of the system and the cantilever. Dominant frequency peaks were observed in the system at 120 Hz and higher harmonics. Example dominant peaks observed in a 30-second recording of a dish with EBS only (baseline).

2.4.2 Determining the presence of vibration in cell cultures: "Catching the fish"

Having calibrated the AFM setup and identified external sources of vibration, we tested the utility of the contact-free AFM method by examining the fluctuation of P0 rat hippocampal pyramidal neurons cultured for one or two weeks. For each cell culture experiment, the cantilever tip was positioned at ~15 μm from the bottom surface of dishes used, which is schematically depicted in Figure 2.1B in the section Methods and Materials. Force fluctuations sensed by the AFM probe were logged for cells under resting conditions, and compared to cells treated with 1 mM cytochrome oxidase inhibitor NaN_3 to block mitochondrial activity. We chose this experimental paradigm as the magnitude of cell oscillations linked to metabolic activity (5,6,16).

Representative cantilever deflection traces are depicted in Figure 2.6A. Granular neurons in cerebellar cultures gave a similar result (n=3), Figure 2.7B. Live untreated hippocampal neurons showed an average RMS value of 1.09 ± 0.062 nm (n = 27 neurons) compared to NaN_3 treated [0.36 ± 0.038nm (n = 12 neurons)] and a baseline empty dish, containing only EBS [0.44 ± 0.007 nm (n = 9 dishes)], Bar graph Figure 2.6C. Representative cerebellar neurons in culture are shown in Figure 2.7A. FFTs were performed on each of the recorded signals to identify patterns in the mechanical oscillations. Representative frequency spectra are shown in Figure 2.6B. No dominant peaks were apparent in the frequency range observed for neurons cultured for one week. Although this was surprising, given neuronal and synaptic activity is the primary source for metabolic activity in neurons, we attributed this finding to the immaturity of network complexity, and low synaptic communication in these cultured cells at one week *in vitro.* However, this assumption needs testing in future experiments.

We expanded our study to measure cellular vibration in pyramidal neurons in more complex networks and mature cultures, where we expected to see increased metabolic activity and neuronal synchronicity. We increased the density of the original, sparsely-seeded cultures, as this is known to improve the rate of spontaneous neural activity (35). Representative images of hippocampal cultures used for vibration recordings at one and two weeks in culture are depicted in Figure 2.8A. We found ~10 % of neurons cultured for two weeks demonstrated a ~3.4 Hz major frequency peak, Figure 2.8C. Interestingly, this result correlated with the observation that some neurons in cultured networks at resting state spontaneously fired with synchronicity given time to mature (35,36). Similarly, the RMS of cantilever deflections was higher for neurons grown for two weeks (n=3) as compared to one-week-old cultures (n=3), Figure 2.8B-Bar graph. These data

describe an ultrasensitive, label and contact free method to monitor cellular oscillations in neurons, and demonstrate for the first-time that neurons in culture vibrate with a specific frequency.

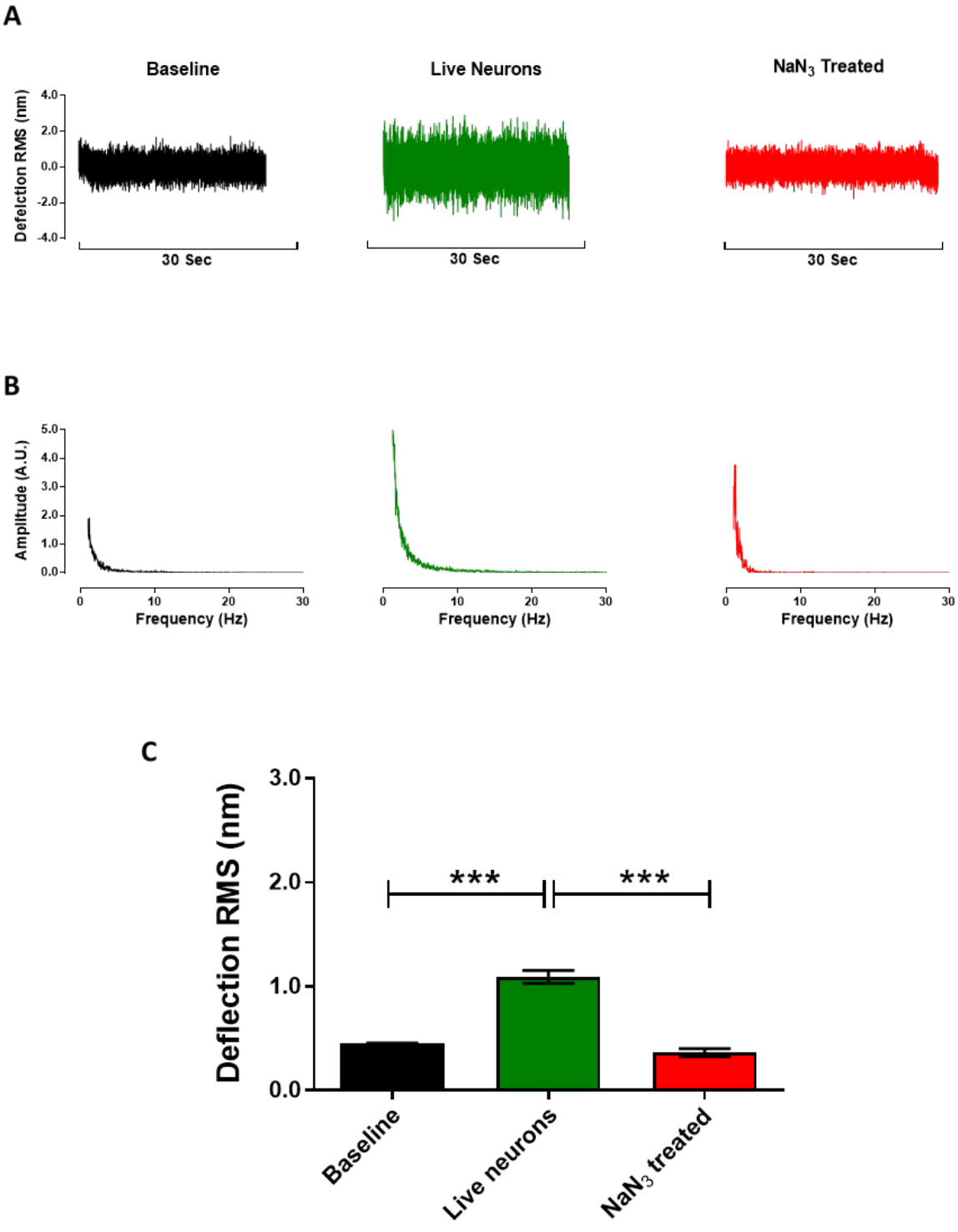
A
Baseline
Live Neurons
NaN3 Treated
Defelction RMS (nm)
4.0
2.0
0.0
-2.0
-4.0
30 Sec
30 Sec
30 Sec
B
Amplitude (A.U.)
5.0
4.0
3.0
2.0
1.0
0.0
0
10
20
30
Frequency (Hz)
Frequency (Hz)
Frequency (Hz)
C
Deflection RMS (nm)
3.0
2.0
1.0
0.0
***
***
Baseline
Live neurons
NaN3 treated

Figure 2.6: Representative time-domain deflection frequency spectrum plots. In (A) empty dish containing no cells (baseline recording), hippocampal neurons grown in culture for one week at resting state, and hippocampal neurons treated with sodium azide are shown. Sample Fast Fourier Transform (FFT) plots for each corresponding condition are shown (B). The deflection RMS for each condition is quantified in the bar graph to the right (C). FFT powers are represented as arbitrary units (A.U.). Bars in deflection plots represent mean RMS values ± SEM. * represents $p < 0.001$ Tamhane post hoc test.**

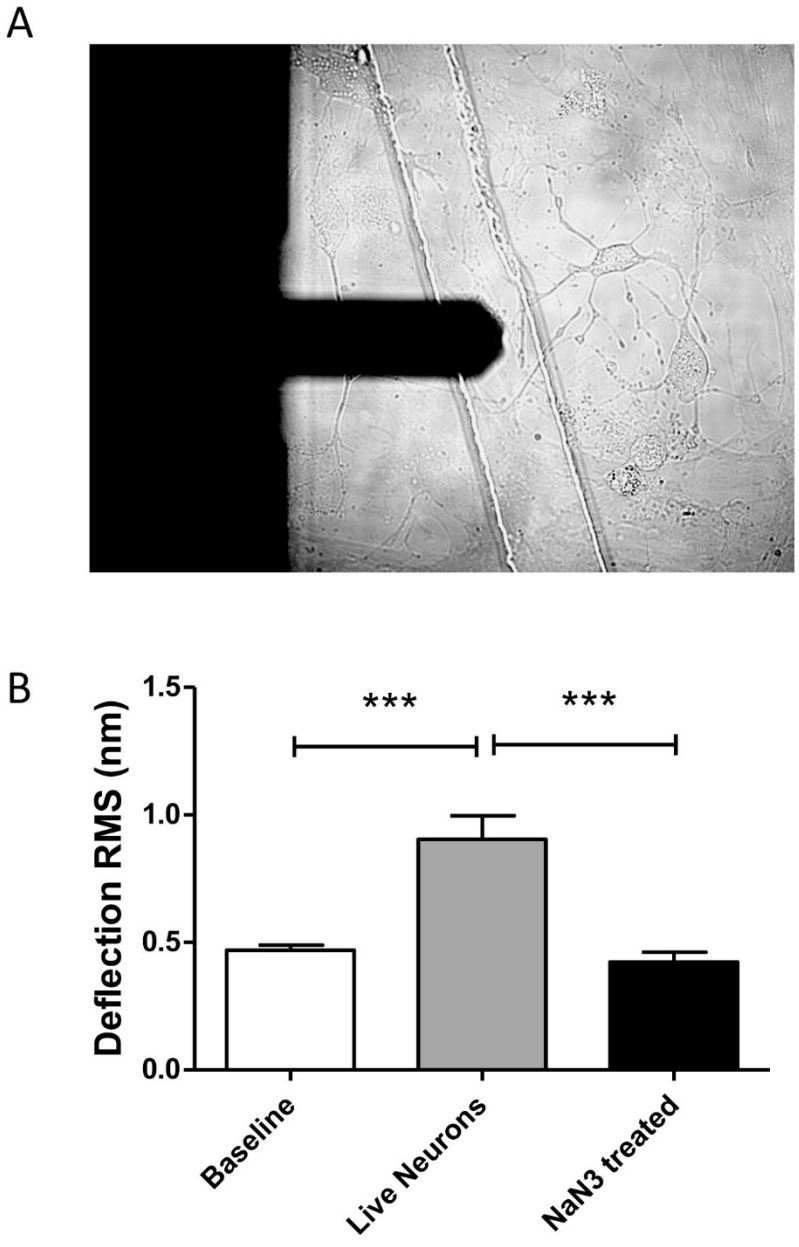

Figure 2.7: Time domain RMS analysis of cerebellum neurons. (A) Sample image of cerebellar cultures used for recordings. (B) RMS amplitude of cerebellum neurons was significantly higher than both 30 min, 1mM sodium azide treated neurons and no-cell recordings. * represent Tamhane post hoc significant differences between groups ($P < 0.001$). Error bars are shown as standard error of mean (SEM)**

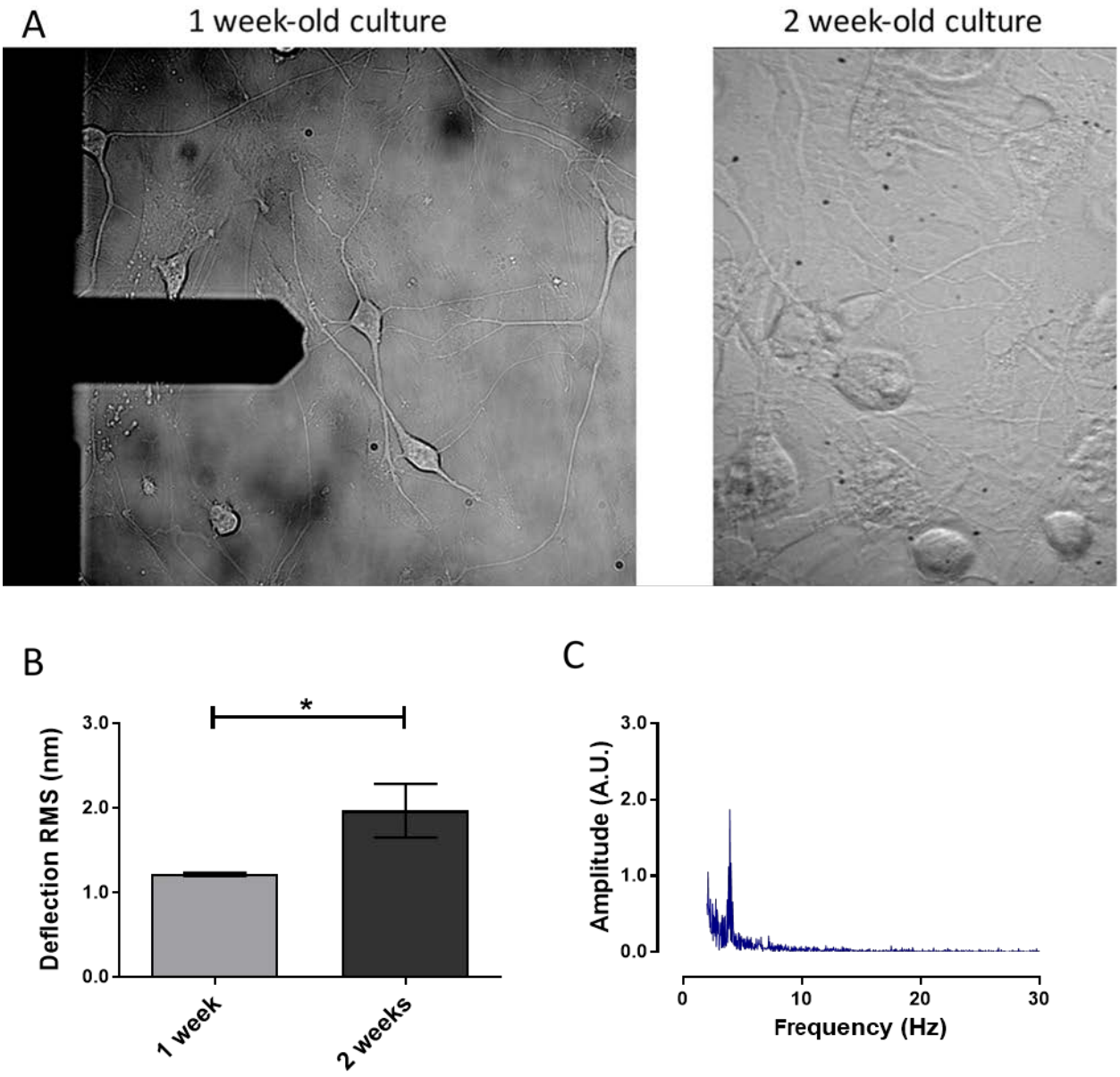

Figure 2.8: Representative images of hippocampal cultures used for vibration recordings at one and two weeks in culture. At two weeks, cultures are denser and neurons form many more connections with surrounding cells. Neural networks are more mature. An increase in cell vibration for neurons cultured from one to two weeks is evident in the quantified RMS bar (C: lower panel). A major frequency peak at ~3.4Hz was present in hippocampal neurons in two week-old cultures (top panel). FFT powers are represented as arbitrary units (A.U.). Bars in deflection plots represent mean RMS values ± SEM. * represents $p < 0.001$ Tamhane post hoc test.**

2.4.3 Assessing AFM system capability to detect vibration at the tissue level

Neurons in complex networks, as in brain tissue, behave differently and demonstrate more synchronized firing than neurons in cultured networks (37). With the establishment of this characteristic neuronal vibration profile in cultured cells *in vitro*, the next step was to investigate this behavior at the tissue level. Accordingly, building on the promising results in neuronal cultures, we examined force vibrations resonating from tissues that were used for corresponding cell culture preparations. For each experiment approximately 8×10^6 μm^3 pieces (W, L, H ~ 200 µm each) were excised from the hippocampus or cerebellum of newborn rat brains, taking care to maintain consistent tissue dimensions.

For each tissue vibration experiment, the cantilever tip was positioned at a distance of ~ 15 µm from the bottom surface of the dish and ~ 5 µm laterally displaced from tissue samples (Figure 2.1B). We conducted a sensitivity study implementing the Stokes Law of vibrational wave attenuation on a range of cantilever-tissue gap, with distances from contact to 5, 10, and 15 µm using the assumption of Newtonian medium and planar wave propagation occurring from the tissue to the cantilever. Stokes Law of attenuation is a formula used to estimate and quantify the decrease in amplitude of propagating vibration waves in liquid media (38). A sample theoretical attenuation calculation is shown in Appendix A, where the rate of attenuation was denoted by α; η estimated dynamic viscosity coefficient of the fluid; ω was the frequency of vibration; ρ was the fluid density estimated as density of water in this case; ν was speed of sound in the fluid; and *d* represented the distance separation between the cantilever and tissue. Given $\eta = 1 \times 10^{-3}\ Pa.s$, $V = 1500\ m/s$ and $\rho = 998.2\ {}^{kg}/_{m^3}$, and given a constant frequency, and substituting the Stokes' attenuation

rate ($\alpha = \frac{2\eta\omega^2}{3\rho V^3}$) , it was calculated to be α =($2 \times 10^{-15} - 1 \times 10^{-14}$). The rate was quite small, and in $A(d) = A_0 e^{-\alpha d}$Ad=e-αd negligible Stokes' rate caused the exponential coefficient to be very close to one, and therefore, we would not expect significant attenuation of the vibration amplitude measured in RMS, recorded over the 15 μm distance.

Importantly, experimental tests using the AFM setup for the distances evaluated above (0-15 μm) demonstrated no significant attenuation to the RMS of the time domain values or a change to frequency patterns for any of the non-contact gap distances when compared to the classical, cantilever-sample contact approach (Figure 2.9 A & B). Indeed, confirmation that the experimental setup was detecting planar wave propagation was expected, given that the ratio of tissue dimensions to the distance between the tissue and cantilever was considerably high. We confidently ruled out spherical wave propagation and dissipation of intensity over the distances and position of the cantilever with respect to sample used in this setup.

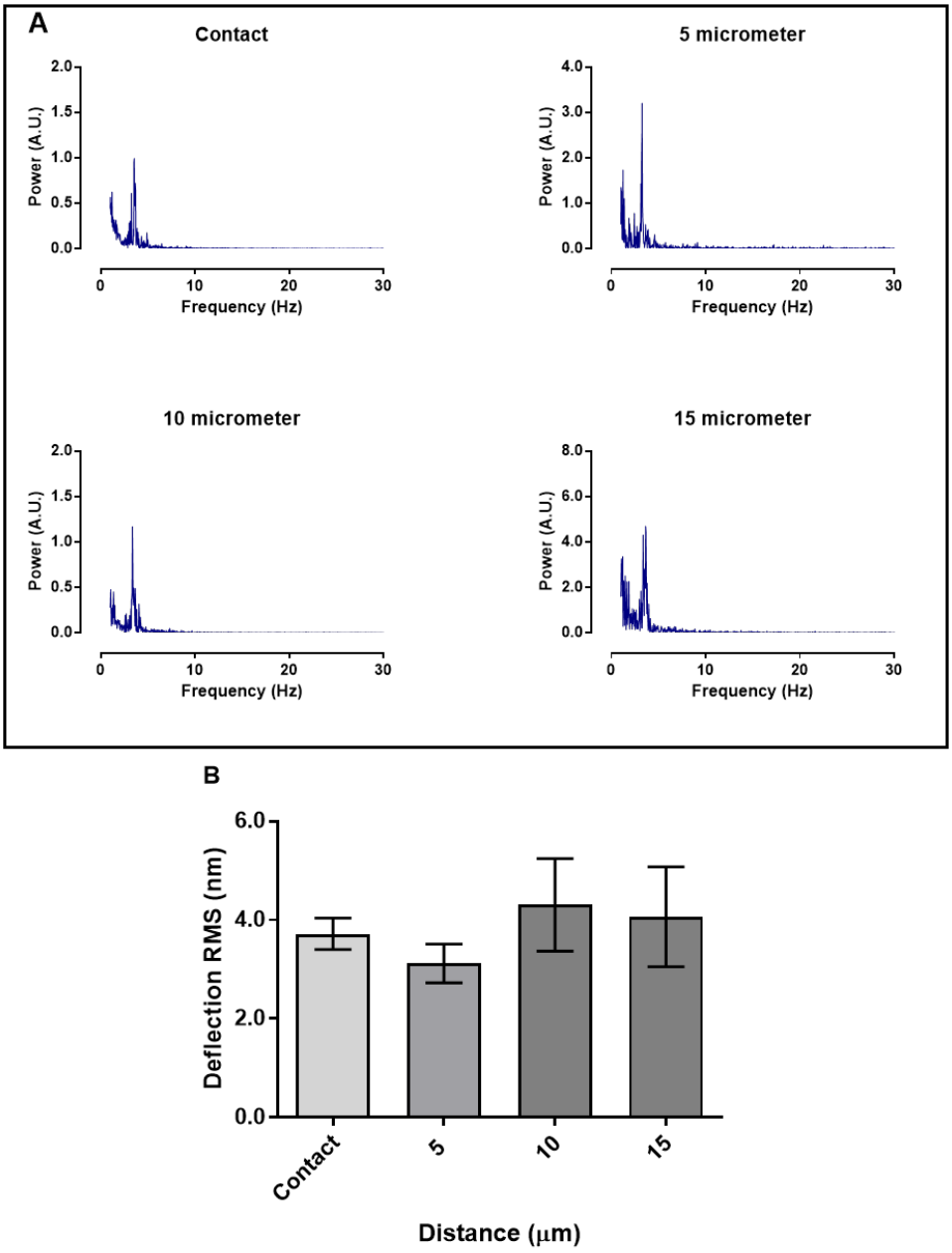

Figure 2.9: Effect of cantilever-tissue distance on the signal attenuation in time and frequency domains. (A) The dominant frequency peak at ~4 Hz did not shift while the cantilever moved up from the contact (0.25 nN) state to 5, 10, 15 µm. (B) The RMS values of the time domain signal did not significantly differ between tested cantilever-sample distances. Bars represent mean RMS values. Error bars are shown as standard error of mean (SEM). Powers of dominant frequency peaks are represented as arbitrary units (A.U.).

Using the above parameters for measurement, hippocampal tissue had a higher basal activity RMS (2.49 ± 0.19 nm, n = 43) of fluctuations (Figure 2.10A bar graph), compared to cerebellum tissue (2.10 ± 0.37 nm, n = 14), Figure 2.10B bar graph. Additionally, FFT revealed a major peak at ~3.4 Hz in hippocampal tissue, but not in cerebellum (Figure 2.10 A&B). As predicted, RMS values for tissues were higher (+ 228 % for hippocampus, + 233 % cerebellum) when compared to cultured neuron deflection RMS data at resting state ($P < 0.001$, Tamhane test). No ~3.4 Hz peak was detected in hippocampal tissue fixed with 4% PFA, or for a non-biological compound of comparable stiffness to brain tissue (1% agarose gel). Nor were RMS values comparable to live tissue in these two cases (Figure 2.11 A&B).

These results confirm the contact-free AFM method is capable of recording vibration force patterns in neural tissue according to brain region with high reproducibility. This method can also identify specific frequency peaks in live tissue that are associated with biological activity, which was demonstrated by the ~3.4 Hz major peak observed in rat hippocampus.

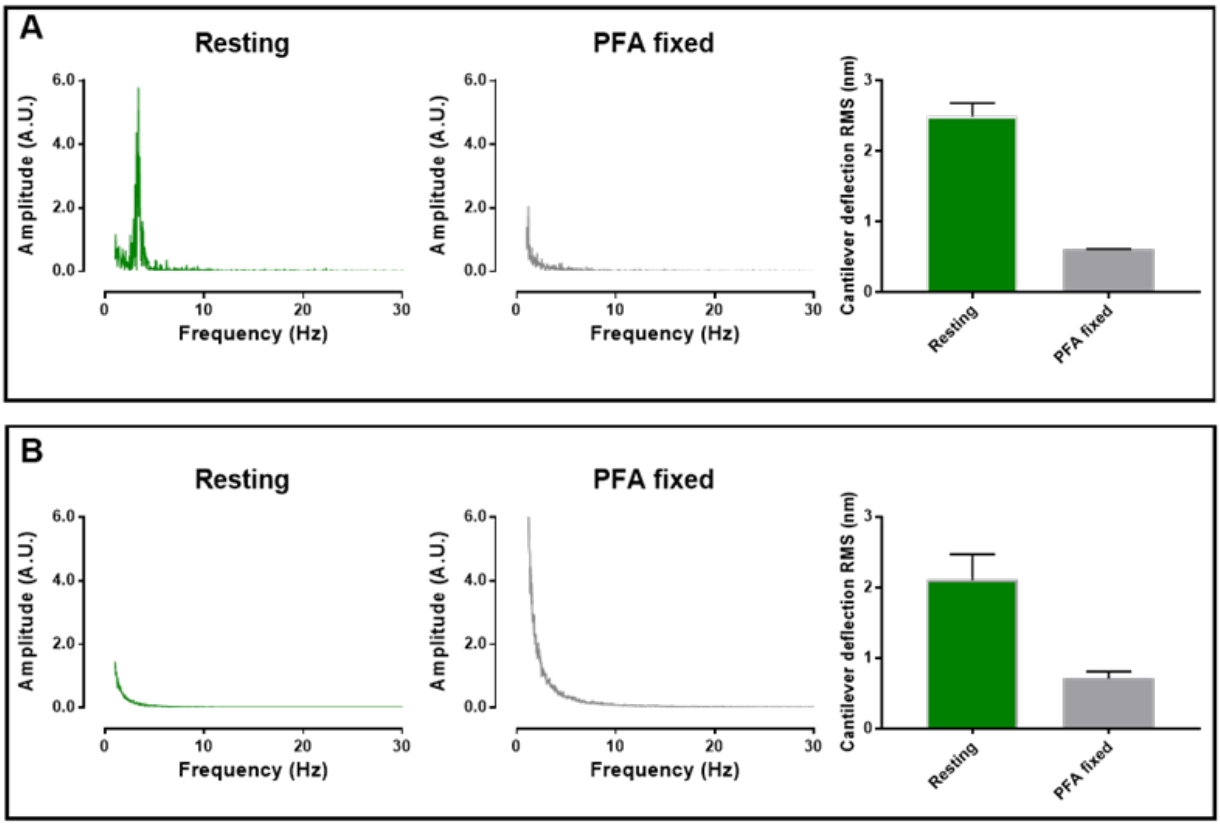

Figure 2.10: Brain region specific tissue vibration. (A) Frequency power spectra of hippocampal tissues in resting conditions and after PFA treatment. A ~4 Hz dominant peak is present for hippocampal tissue in the resting state. (B) No ~4 Hz dominant peak was present in cerebellum at resting state. RMS calculation corresponding to the two brain regions are shown as a bar graphs.

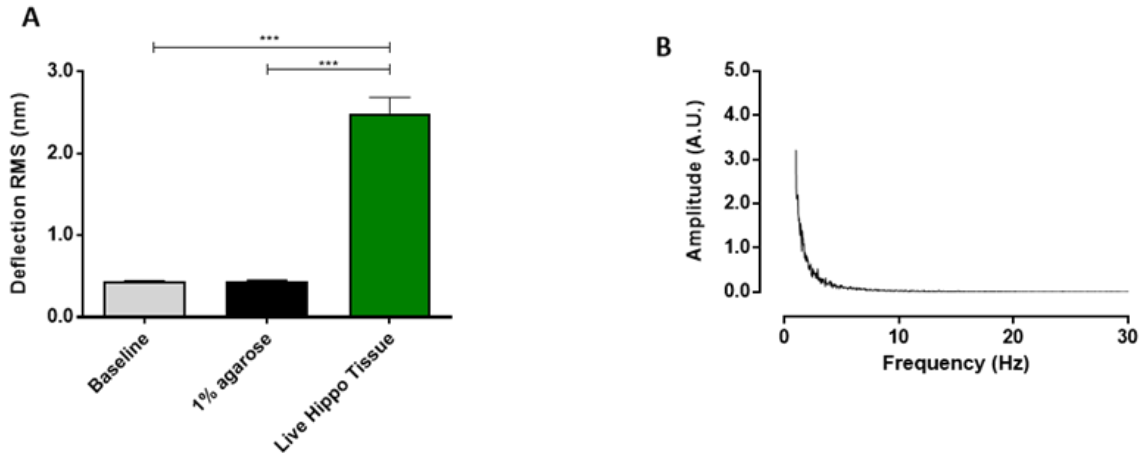

Figure 2.11: Comparison of vibration patterns between live neural tissue and agarose gel. (A) RMS vibrational amplitude of 1.0 % agarose gel is similar to no cell RMS vibration, and it is significantly different from resting hippocampal tissue RMS. Bars represent mean RMS values ± SEM. * represent Tamhane post hoc significant differences between groups ($P < 0.001$). (B) Frequency pattern of 1.0 % agarose gel is shown. The ~4 Hz dominant frequency observed in resting hippocampal tissue is absent for 1.0 % agarose gel. Powers of dominant frequency peak is represented as arbitrary units (A.U.).**

2.4.4 Effect of chemical reagents on vibration

In these experiments, we explored the potential of AFM for studying the effects of pharmacological agents on vibration. We also investigated the source of the 3.4 Hz peak observed in the excised hippocampal tissue at resting state. Our goal was to test the potential of the AFM system as a real-time, drug-testing platform.

In the first experiment, rapid neuron firing was triggered by the transfer of tissues at resting state (EBS only) into a high-K^+ buffer. High-K^+ depolarization of hippocampal and cerebellum tissue increased the mean RMS to 3.31 ± 0.503 nm (n = 22), and 2.61 ± 0.289 nm (n = 7) respectively (Figure 2.12 B&D). The ~3.4 Hz major frequency peak remained present in the FFT of depolarized hippocampus, but more interestingly, a ~3.4 Hz major frequency peak was now present for depolarized cerebellum that had been absent in the resting state (Figure 2.12 C). We next blocked neuronal activity using two pharmacological methods (removal of extracellular Ca^{2+} or incubating tissue with 1μM Tetrodotoxin (TTx)) and studied the effect on tissue vibration. In both conditions, the ~3.4 Hz major peak present in the depolarized tissue frequency spectrum disappeared (Figure 2.12 A &C). Similarly, RMS values decreased [hippocampus; Ca^{2+}-free: 1.32 ± 0.21 (n = 8), TTx: 0.97 ± 0.362 nm (n = 22), cerebellum; Ca^{2+}-free: 1.42 ± 0.32, TTx: 0.99 ± 0.013 nm (n = 6)] (Figure 2.12 B&D). These experiments connect the ~3.4 Hz peak to neuronal firing in tissue, and although this result will require further justification, using another technique such as electrophysiology, it demonstrates the potential of the system to investigate cellular mechanisms, and the further clinical importance of the system as a real-time drug testing platform

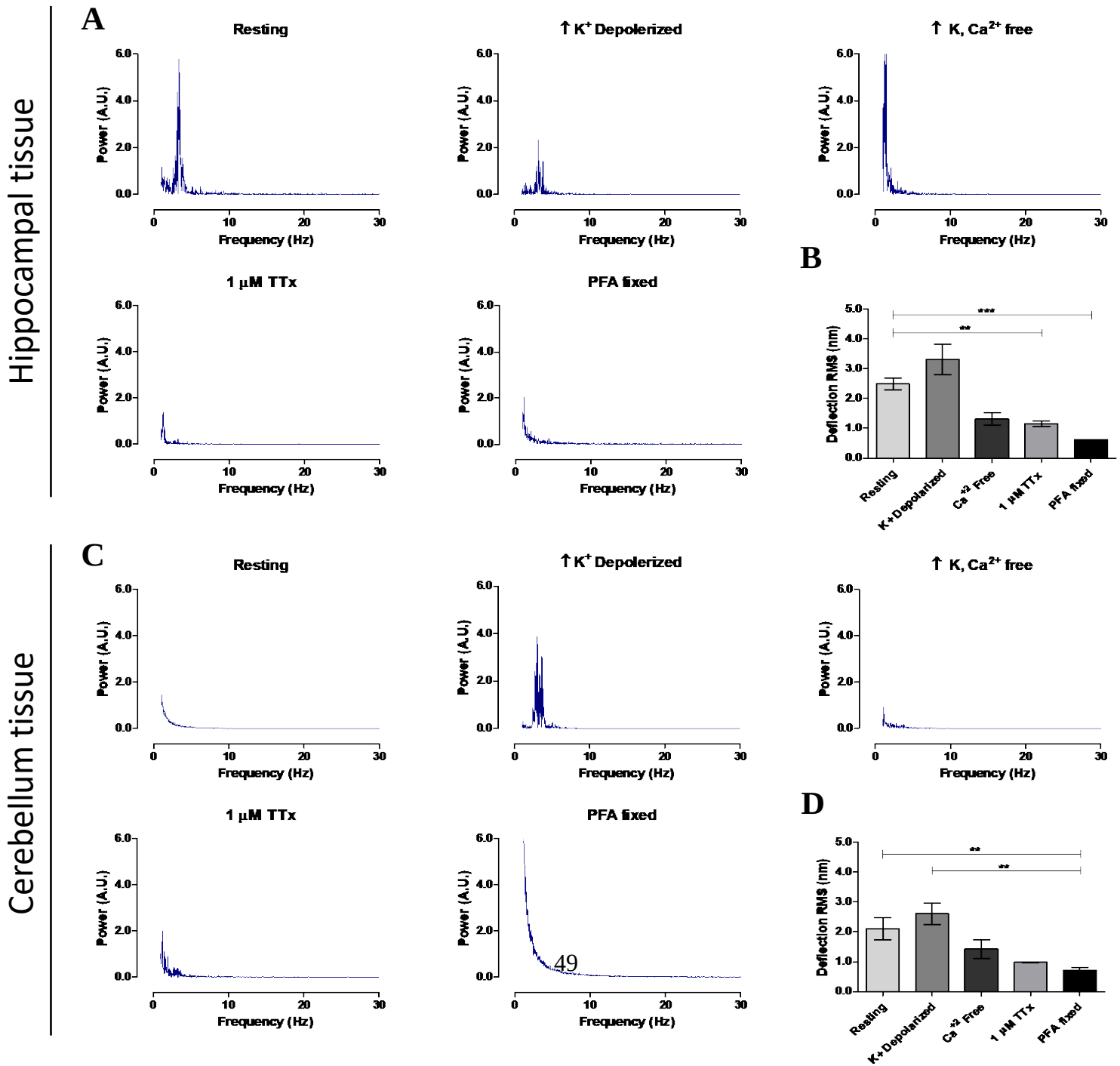
Hippocampal tissue
A
Resting
↑ K+ Depolerized
↑ K, Ca2+ free
1 µM TTx
PFA fixed
Power (A.U.)
Frequency (Hz)
B
Deflection RMS (nm)
Resting
K+ Depolarized
Ca +2 Free
1 µM TTx
PFA fixed
Cerebellum tissue
C
D

Figure 2.12: Brain region specific tissue vibration patterns. Representative frequency spectra for hippocampal tissues (A) and cerebellum tissues (C), according to treatment conditions as labeled (resting, high K+ depolarization, high K+ buffer without Ca2+, 30 min 1 µM TTx treatment and 4% PFA fixation). (B and D) Representative time-domain deflection plots for each condition are quantified in the Bar Graph B - hippocampus and D - cerebellum. Power of frequency spectrum is represented as arbitrary units (A.U.). Bars in deflection plots represent mean RMS values ± SEM. * and ** represents $p < 0.001$ and $p < 0.01$ respectively, Tamhane post hoc test.**

2.4.5 Discussion & conclusion

The study of cellular activity and membrane fluctuation through nano-mechanical oscillation with AFM remains an emerging field, and measurement of cell vibration has been restricted previously to single cells. Recently, single prokaryotic and eukaryotic cells were shown to mechanically oscillate as detected by the cantilever of an atomic force microscopy (AFM) (5,7,39). Importantly, the magnitude of these nanoscale fluctuations was shown to be linked directly to a cell's metabolic activity (5). Therefore, we hypothesized that this phenomenon observed for single cells could be applied to detecting vibrational signatures in cells in culture and at the tissue level. Therefore, we custom-developed a contact- free AFM method to measure mechanical oscillations in both cells in culture, and tissues excised from the developing rat brain. The complete AFM setup used in our study is detailed in (Figure 2.1).

The results in this chapter demonstrated the method developed to be a successful technique to record biological activity of brain cells and tissues, without direct physical interaction. Vibration recording might prove a useful technique to study healthy brain function and neural networks. In the rat brain, neuronal firing rates differ substantially between brain regions and development. In newborn rats, the hippocampus is intrinsically more active than the cerebellum as a function of limited neuronal architecture at this time point in the development of the cerebellum, whereas, some of the pyramidal cell circuitry in the hippocampus is established (40-43). Therefore, we hypothesized that if this system could detect neuronal activity-derived patterns in vibration, then these two brain regions would be ideal to identify differences. Indeed, this is what we observed, in both hippocampal cultures and tissue: We found a major frequency peak was present, but no major frequency peak was identified in a cerebellar sample unless it was chemically depolarized.

A ~3.4 Hz peak was observed in the hippocampal samples. Interestingly, this correlates with reported high amplitude theta oscillations in the hippocampus of neonatal rat pups (44-46) which have been detected even as early as two-days old (47). Conversely, very little is reported on spontaneous synchronized cell firing within the cerebellum of newborn rat pups. Synchronous firing in the cerebellum requires Purkinje cell innervation by climbing fibers and inferior olivary cells (48,49) and at P0, these connections have not formed; development of Purkinje cells does not really begin to accelerate until P12 (40). This might offer an explanation for no peak in the frequency spectrum. Further, the neuron-glia co-cultures used in this experiments are well established and used in a number of publications by our group and collaborators (95-98). Prior to this study, calcium imaging was used to approximate synchronous firing rates of these cultures at the same time point in maturity that was used in this report (99). This study showed synchronous bursting of neuron networks in cultures to be <10 Hz in the range of our reported vibration peak.

Similar firing rates (1-5 Hz), have been reported in cortical cultures by other groups (100).

In addition, El Hardy et al 2015 presented an experimental and theoretical model demonstrating the electrical component of an action potential in a single neuron is accompanied with a mechanical membrane surface, wave-driven by travelling axoplasmic fluid propagation (19). Such mechanical waves could be responsible for displacement measured by the cantilever in these brain regions and in neuron cultures. However, it should be noted that the contribution of other cells, such as astrocytes, or additional mechanisms present in cultures and tissues, that include astrocytic calcium wave propagation in observed vibration, has not been investigated and might also explain the differences observed between brain regions.

On the other hand, RMS might be a more effective measure of overall neuronal activity with its additional capacity to detect non-synchronous neuronal firing. Interestingly, when activity was blocked by treating tissues with TTx, a decrease in RMS of 80% from resting state was observed for both brain regions. Importantly, this is the same percent contribution reported for total brain metabolism attributed to neural activity, and further supports the idea that RMS levels are correlated to metabolism (50), and in the brain, this is primarily a result of neural activity. It will be important to confirm these theories by adjuvant techniques, such as electrophysiology and metabolic characterization.

Having demonstrated the method we developed to be a successful technique to record biological activity of cells and tissues without direct physical interaction, this technique may be used to investigate biological mechanisms in their natural state. This would perhaps be preferable to current techniques, such as electrophysiology, or patch clamp, that require interaction with cell membranes, and risk potential damage to cells. Any cell damage can interfere with subsequent

recordings, or other molecular-based sensors, such as, cell loading with calcium indicators, or over-expression of metabolic activity sensing proteins. Furthermore, this new AFM technique is capable of studying the close relationship between brain synaptic activity and overall cellular metabolism, which is difficult to achieve using existing technologies. In addition, learning that different regions of the brain appear to display unique vibrational profiles, prompts us to speculate that this technology can be used to diagnose brain injuries. We envision variants of this method to be of importance in the clinical diagnosis of metabolic disturbances by identifying metabolically pathological tissue, such as brain tumors.

Chapter Three: **Ultrasensitive methods to characterize human brain tumor cells and tissues based on distinct vibration profiles**

3.1 Introduction

Research on new methods to detect cancer, and efforts to develop novel techniques for clinical diagnostics are evolving (15,51). For example, the stiffness of cancerous cells and tissues is under investigation as a possible biophysical property to detect and diagnose cancer. Magnetic resonance elastography studies, for instance, have shown that cancerous tissue is stiff, compared to surrounding healthy brain tissue, and that the magnitude of this textural difference may be an indicator of cancer progression (52). At the cellular level, magnetic bead twisting (53) and optical tweezers (54) have been implemented to evaluate differences between healthy and cancerous cells (55). Cell stiffness has also been used as a means to distinguish metastatic cancer cells *ex-vivo* using contact-mode AFM (56,57). While each of these techniques has shown promise in differentiating tumor and brain cells, the utility of these techniques is extremely limited because current techniques require each cell to be probed individually. Additionally, stiffness values can vary considerably across the surface of cells and tissues (58-60).

On the other hand, a unique signal, intrinsic to the whole sample, could be attained by characterizing the specific oscillations emitted from cells and tissues. Moreover, results from the previous chapter suggest that cellular vibration contains information about the identity and function of biological samples when recorded using the contact-free AFM technique. This newly-developed vibration detection technique was assessed using samples obtained from animal models; the results indicated that the intensity of fluctuations measured in RMS may be linked to the overall metabolic status of the cells. This critical finding is in agreement with previous AFM-based vibration studies (5,61), where RMS was reduced significantly for cells in culture after treatment with the mitochondrial inhibitor, sodium azide. Accumulating evidence also suggests studying the

metabolism of tumors is important in cancer research because cancer cells have an altered metabolism, due to unregulated cell proliferation. Understanding the affected mechanisms might offer new ways of treating cancers (62). Therefore, identifying cancers using their vibrational profiles could prove to be an important tool in cancer screening and diagnosis.

This idea prompted us to further investigate whether vibration could distinguish between healthy and cancerous cells. Specifically, in this section of the thesis we evaluated if the intensity of fluctuation and spectral analysis could discriminate cancerous cells and tissues.

The experiments described in this chapter have two main objectives: First, at the cellular level, that included cultured and single cells, we explored the potential of the AFM and optical tweezers (OT) systems to distinguish between cancerous cells based on their vibrational profiles, i.e. RMS and frequency spectrum. Cellular vibrational occur as membrane deflection in the order of less than 10 nanometre range (5,6). Subsequently, these faint cellular vibrations are beyond the reach of the current optical imaging systems. Super resolution light microscopes such as STORM, PALM and NSOM at best have spatial resolution of 20 – 30 nanometers (94), and the process of acquiring images may provide inefficient and insufficient temporal resolutions to capture the fast-occurring fluctuations. On the other hand, imaging systems such as electron microscopy provide the best spatial resolutions but are not suitable for capturing live cell images (101). As a result, we resorted to making the necessary modifications to utilize AFM and OT's exceptional instantaneous nanoscale force detection capability to capture tissue vibrations. In the first objective using these two technologies we examined an aggressive glioma cell line (U178), cells from a slow growing brain tumor (BT048), and human fetal astrocytes (HFA). The latter is a common control cell line for brain tumor research. Second, we assessed the AFM system's capability to distinguish brain

tumors at the tissue level. We examined this second objective using fresh brain tumor biopsies obtained from the operating room.

The preliminary results revealed the clinical potential of the methods to differentiate various brain tumors from normal tissue on the basis of vibrational profile. Cultured brain tumor cells were distinguishable based on the overall metabolic activity of cells, which appeared to be associated with the vibration amplitude measured in RMS. We were able to demonstrate the vibration detection sensitivity of the OT system through rich and unique frequency spectrum cells that were not apparent in the AFM method. As well, at the tissue level, malignant astrocytoma samples obtained from the operating room -- transported in artificial cerebrospinal fluid, and tested within an hour -- vibrated with a much different frequency profile and amplitude than meningioma or lateral temporal cortex. This provided us with a quantifiable measurement to accurately distinguish the three tissues in real-time. We have also described a method to convert oscillation signals into sound within the frequency range of human hearing. Overall, this chapter presents data and novel concepts that could translate, potentially, into the development of a tool for the rapid discrimination of cancerous cells in a clinical setting.

3.2 Methods and Materials

3.2.1 Experimental design, methods and analysis

The experimental setup consists of either an atomic force microscope (NanoWizard® II AFM, JPK Instruments AG, Germany) for cultured cells and tissue interrogations (Figure 2.1) or optical tweezers (NanoTracker®, JPK Instruments AG, and Germany) for single cell studies (Figure 3.1). The RSA5103BF spectrum analyzer (Tektronix Inc.) was provided by the Arnie Charbonneau Cancer Institute. We used the spectrum analyzer to assess the stability of the signal being recorded and to determine the sampling rate for offline analysis. For all experiments, three 30-second segments of vibration signals were recorded. Independent experiments were performed on at least three separate biological preparations. Our data analysis of the vibration signal in the time domain (RMS) is described in Chapter 2, The frequency analysis (i.e. FFT) compared the magnitude and frequency patterns of the signals, using a custom- written MATLAB algorithm (Appendix B). Using one-way ANOVA, we compared mean RMS amplitudes in cases where more than two data groups were present. N-values represent biological replicates carried out for each cell-line, primary culture or tissue preparation. Tamhane post hoc analysis was used to determine statistical significance. Independent t-tests were used to compare mean RMS amplitudes where differences between two groups were analyzed.

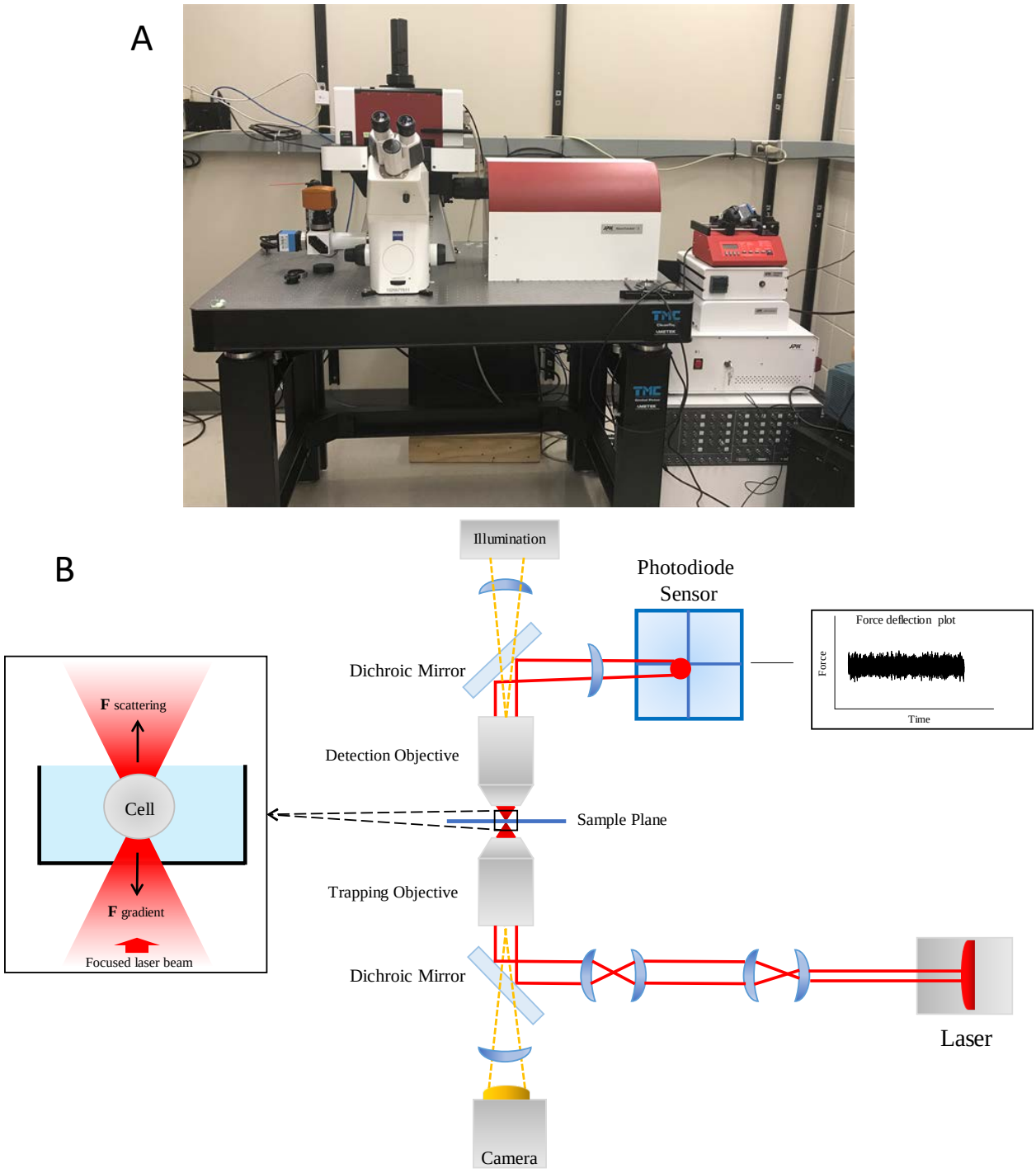

Figure 3.1: Optical tweezer based experimental setup for single cell vibration study. (A) Picture of JPK NanoTracker®. Panel (B) depicts schematic representation of the optical tweezers, where a cell is suspended in the laser focus center. Three dimensional cellular movements are detected as force and/or displacement deflections by a four-segment photodiode. Image is modified from JPK NanoTracker manual user.

3.2.2 Brain tumor cell line preparation and vibration recording

We prepared and maintained U178 cells in MEM supplemented with 10% fetal bovine serum (FBS) as per (63,64). Human fetal astrocytes (HFA) were prepared and cultured as per Lawrence et al (65). We cultured BT048s, a BTIC line, from a resected specimen of a patient's malignant glioma, according to Sarkar et al (66). We analyzed the vibrational profiles of fast-growing glioma cell line (U178, n = 16), slow-growing brain tumor initiating glioma cells (BT048, n = 18) and human fetal astrocytes (HFA, n = 18), a common control cell line for brain tumor research. Brain tumor cells were grown in neurosphere human media with the addition of epidermal growth factor (EGF), fibroblast growth factor (FGF), and heparin. The cells were passaged when the clusters of cells are about 200-400 microns in size. The cells were spinned at 700 RPM for 10 minutes and excess media aspirated. Then, 1 ml of Accumax enzyme (Innovative Cell Technologies cat # AM105) is added and incubated at 37ºC for 8-10 mins. About 8 milliliters of media (Gibco 10XDMEM cat # 12100-046 / F12 Cat #21700-075) was added and spinned at 700 RPM for 10 mins. The media was aspirated, and the cells are resuspended in 1 milliliter of media. The cells were seeded at 200,000 cells in a T25 flask. The cells were maintained with about 2 milliliters of fresh media and cultured for one week.

For AFM vibration recordings, we seeded 50 000 cells/well of the recording petri dish and allowed cells to attach and grow for 24 h. Individual cells were suspended at the focal spot of the OT system single cell vibration recording and analysis. All vibration recordings were taken for each cell line following replacement of growth media with an EBS recording solution.

3.2.3 Tumor cell oxygen consumption rate analysis

Oxygen consumption rates (OCR) of the above prepared tumor cells in culture were measured using the Seahorse XF24 Extracellular Flux Analyzer (Seahorse Bioscience, Billerica,

MA), according to the manufacturer's instructions. Briefly, 50,000 (HFA, U178 or BT048) cells/well grown on XF24 cell culture microplates were switched to an assay medium (unbuffered DMEM supplemented with 25 mM glucose, 4 mM glutamine, and 2 mM sodium pyruvate), and incubated without CO_2 at 37ºC for 45 min. Next, the mitochondrial function assay was performed with a sequential injection of oligomycin (1 μg/ml; Enzo, Life Sciences, Brockville, Canada), carbonyl cyanide-4-trifluoromethoxyphenylhydrazone (FCCP; 0.5 μM; Sigma-Aldrich), and antimycin A (1 μM; Sigma-Aldrich) at the indicated time intervals.

The XF24 Extracellular Flux Analyzer (Seahorse Bioscience, Billerica, MA) is a fully integrated 24-well instrument that measures in real time the uptake and excretion of metabolic end products. Each XF assay kit contains a disposable sensor cartridge, embedded with 24 pairs of fluorescent biosensors (oxygen and pH), which is coupled to a fiber-optic waveguide. The waveguide delivers light at various excitation wavelengths (oxygen _ 532 nm, pH _ 470 nm) and transmits a fluorescent signal, through optical filters (oxygen _650 nm, pH _ 530 nm) to a set of highly sensitive photodetectors. Each fluorophore is uniquely designed to measure a particular analyte. Optical sensors for oxygen and pH in solid phase on the probe are positioned within the extracellular medium, where they detect real-time changes in oxygen and proton analytes, continuously and reversibly, as cells consume oxygen and extrude protons.

3.2.4 Brain tumor and cortex specimen collection

Brain tumor and cortical tissue specimens were collected from patients during surgical resections by neurosurgeons at the Foothills Medical Centre, Calgary, Alberta. Ethical approval for the collection of human tissues for the study was obtained through the University of Calgary Conjoint Health Research Ethics Board, and informed consent for intra-operative tissue sampling was obtained from all patients prior to inclusion in the study. Protocol number: HREBA.CC-16-

05502 REN2. The University of Calgary Conjoint Health Research Ethics Board also scrutinized each experimental protocol in the study to confirm compliance with institutional guidelines and regulations. Approval was received prior to the commencement of the study. To identify, dissect, and maintain an ideal tumor-brain tissue plane, specimens were obtained from the lesion and sent for histopathology analysis. Additional samples were obtained from the tumor core or lateral temporal cortex during epilepsy focus removal surgery. Samples were transported in artificial cerebrospinal fluid, and vibration analysis was conducted immediately. Following vibration recordings, the tissue was fixed in formalin. H&E staining and imaging was performed on all tissues Additionally, GFAP imaging was completed on the malignant astrocytoma samples.

Table 3.1: Patient information. Description of patient characteristics and pathology.

Case#	Age/Sex	Pathologic diagnosis, grade and/or location
1	44y/M	Astrocytoma WHO Gr 3
2	52y/M	Atypical meningioma WHO Gr 2
3	69y/F	Astrocytoma WHO Gr 4
4	58y/F	Meningioma WHO Gr 2
5	36y/M	Astrocytoma WHO Gr 4
6	47y/F	Meningioma WHO Gr 1
7	40y/F	Mesial temporal epilepsy, specimen - Right lateral temporal cortex
8	28y/M	Mesial temporal epilepsy, specimen - Left lateral temporal cortex

3.2.5 Converting AFM vibration signals to audio waves

As most of the frequency peaks observed were below 20 Hz, playing back the original vibration signal did not provide a distinguishing sound for different cancer types. Therefore, we implemented a frequency modulation method (frequency-shift keying) to transfer the vibration signals (baseband signals) through a sinusoidal carrier to a frequency range above 100 Hz. This sound could then be played back through common, low performance speakers. This approach changed the pitch (frequency) of the audio tones. The technique also provided a stronger signal than the amplitude modulation, as the signal-to-noise ratio is higher in this method. To avoid a clipping effect, the modulated signal was normalized prior to converting it to wave signals.

3.3 Results

3.3.1 Correlating cultured brain tumor cell vibration to metabolic activity

We explored the clinical potential of AFM's contact-free mode vibration detection by first testing its effectiveness in distinguishing between cancer cell lines. We analyzed a fast-growing glioma cell line (U178, n = 16), slow-growing brain tumor initiating cells (BT048, n = 18) and human fetal astrocytes (HFA, n = 18), a common control cell line for brain tumor research. FFTs did not reveal any major frequency peaks for any cell type. However, fast growing U178 cells exhibited significantly higher RMS, compared to slow-growing BT048 and HFA cells (Fig. 3.2D). Accumulating evidence suggests that the magnitude of cell fluctuations reflects overall cellular metabolic activity (5,16). Indeed, we observed a reduction of RMS values in cultured neurons treated with a mitochondrial inhibitor (Fig. 2.3A). However, a direct correlation between metabolic activity and cellular oscillation in untreated cells has not been confirmed. Therefore, we next performed bioenergetics experiments on each cell line using an FX^{e}24 analyzer (Seahorse Biosciences). An example of the experimental workflow and oxidative respiration data is illustrated in Fig. 3.2A. For this study, we were interested in comparing RMS to untreated basal mitochondrial respiration. Untreated U178 cells showed basal metabolic activity ~200% above other untreated cell lines; no differences were observed in oxygen consumption rates between BT048 and HFA cells which agreed with RMS data (Fig.3.2B&C).

We conclude that the contact-free AFM system is potentially useful in indicating the mitochondrial respiration rate of cancer cells in culture with different growth rates, in real-time. However, further cell lines must be tested to confirm whether RMS can distinguish cell lines from one another. We propose cellular vibration could be an important tool for studying metabolism in cancer cell culture models, e.g. monitoring RMS changes of cells in response to drug treatment.

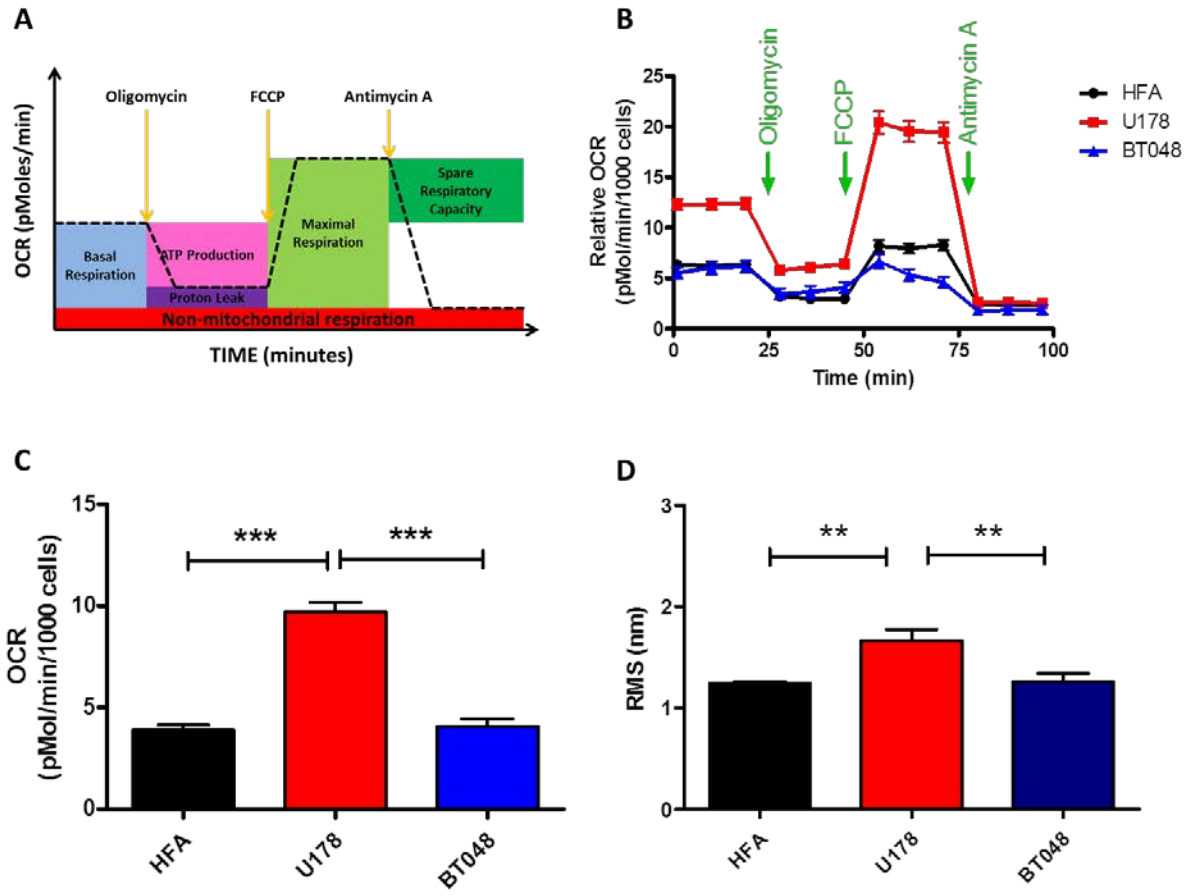

Figure 3.3: RMS correlation with metabolic activity. RMS is correlated directly to metabolic activity (A) Schematic representation of the bioenergic experimental workflow and metabolic data obtained. (B) Oxygen consumption rate (OCR) profiles are shown for each cell line (Fast growing glioma cell line (U178), slow-growing cell line BT048, and human fetal astrocytes (HFA)). Arrows indicate the time of addition of oligomycin (1 µg/ml), FCCP (0.5 µM), and antimycin A (1 µM) to evaluate different states of mitochondrial respiration. Graph shows average of two plates. Each plate has 6-8 replicates. (C) The bar graph shows quantified OCRs (basal respiration) of each untreated cell line. Base OCR data follows the trend observed for the deflection RMS plots. Data are expressed as mean ± S.E.M. (D) Bar graph depicting mean deflection RMS of cultured cancer cell lines. Fast-growing U178 cells have a higher RMS of vibration compared to a slow-growing BT048 cells and HFA cells.

3.3.2 Use of optical tweezers (OT) to characterize individual cancer cells

For any of the three cultured cell lines examined, (U178, BT048, HFA), Fast Fourier Transform (FFTs) analysis did not reveal any major frequency peaks. We attributed this lack of spectral profile in the cultured cells to the AFM probe (cantilever) stiffness and its susceptibility to thermal fluctuations (33), which may have dampened and hindered the vibration. The OT system is well-documented to have superior force detection sensitivity with a much higher sampling frequency rate. Therefore, in this section we assessed the quality and utility of the OT system with respect to the vibrational profiling of human cancer cell lines.

To get a better sense of how phenotyping for cancer diagnosis may work using the OT, we examined brain tumor cancer cell lines corresponding to ones used in the AFM technique. Figure 3.3 shows time-domain amplitude quantified in RMS, and spectral profiles of the single (individual) cells suspended in the laser focus center of the OT system. We examined HFA (n=18) and glioma cancer derivatives, including glioma cell lines U178 (n=34) and brain tumor-initiating cells, BT048 (n=33). In agreement with the contact-free AFM results, a similar RMS trend was noted (Fig. 3.3A). Specifically, significant RMS differences were noted between the aggressive glioma cell line, the slow-growing brain tumor cell line, and human fetal astrocytes (Figure 3A). The U178 cells exhibited higher RMS values (3.89 ± 0.985pN) compared to BT048 (0.12 ± 0.012pN) and HFA (0.14 ± 0.025pN) cells. In addition, overall inspection of the power spectra, with a sampling frequency of 100 KHz, showed both similarities and differences in the frequency domains (Figure 3B). When zoomed into specific frequency ranges, we found some spectral components shared among all cells (Figure 3.4 A); whereas, other regions demonstrated distinct peaks unique to the cell type examined (Figure 3.4B). For example, in all cell types, consistent quadruplet dominant frequency peaks were noted between 16 – 18 kHz. Differences were observed

in the frequency range of 1 – 2 KHz. Two unique frequency peaks were observed at 11.5 and 14 KHz for HFA, and a single frequency peak shifted at 14.5 kHz in U178, while there were no dominant peaks noted in BT048 cells. These findings were consistent among cells from the same source, suggesting that in addition to RMS, spectral analysis might allow phenotyping and the differentiating of human cell types, including those from cancers.

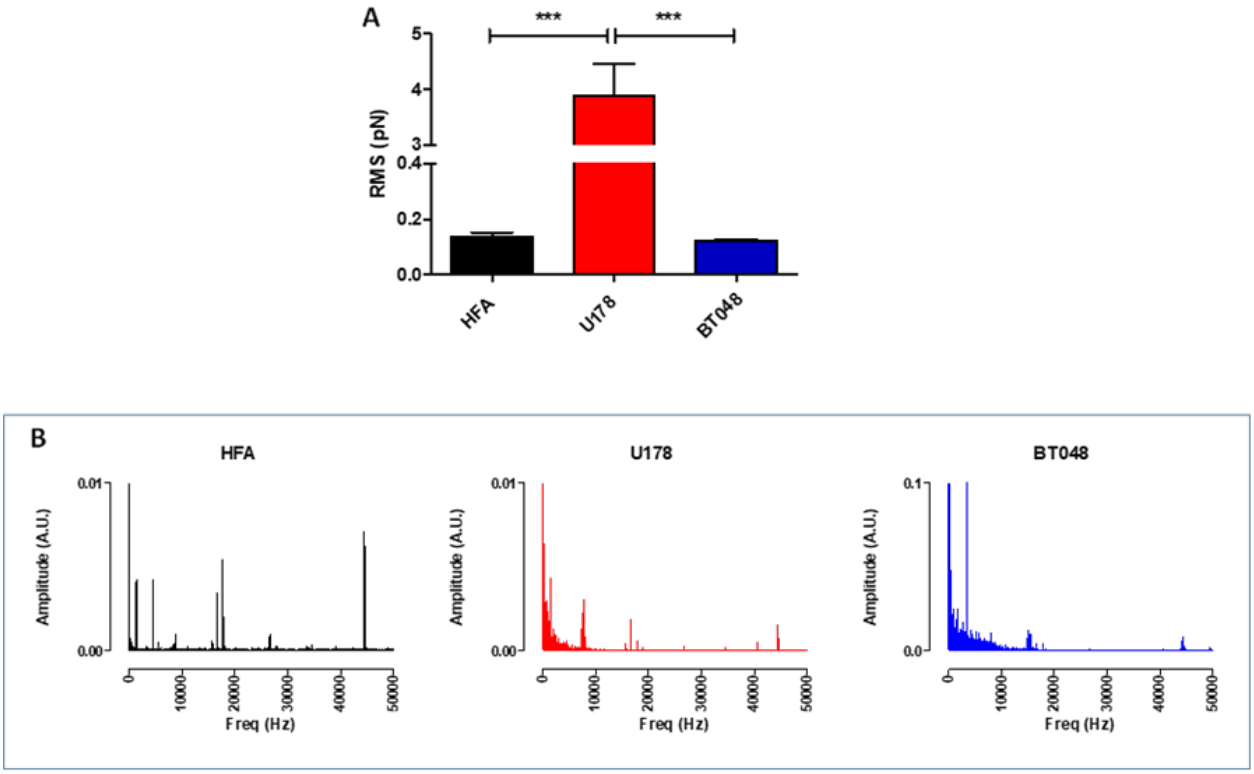

Figure 3.4: Vibrational characterization of single cells using optical tweezers. (A) Bar graph depicting mean deflection RMS of cells quantified as force. In red, fast-growing U178 (n=14) cells show a higher RMS of vibration compared to slow-growing BT048 (n=16) cells and HFA (n=18) cells. As well, the overall appearance of the FFT spectral analysis corresponds to the three cell types shown in Panel B. FFT powers are represented as normalized arbitrary units (A.U.). Bars in deflection plots represent mean RMS values ± SEM.

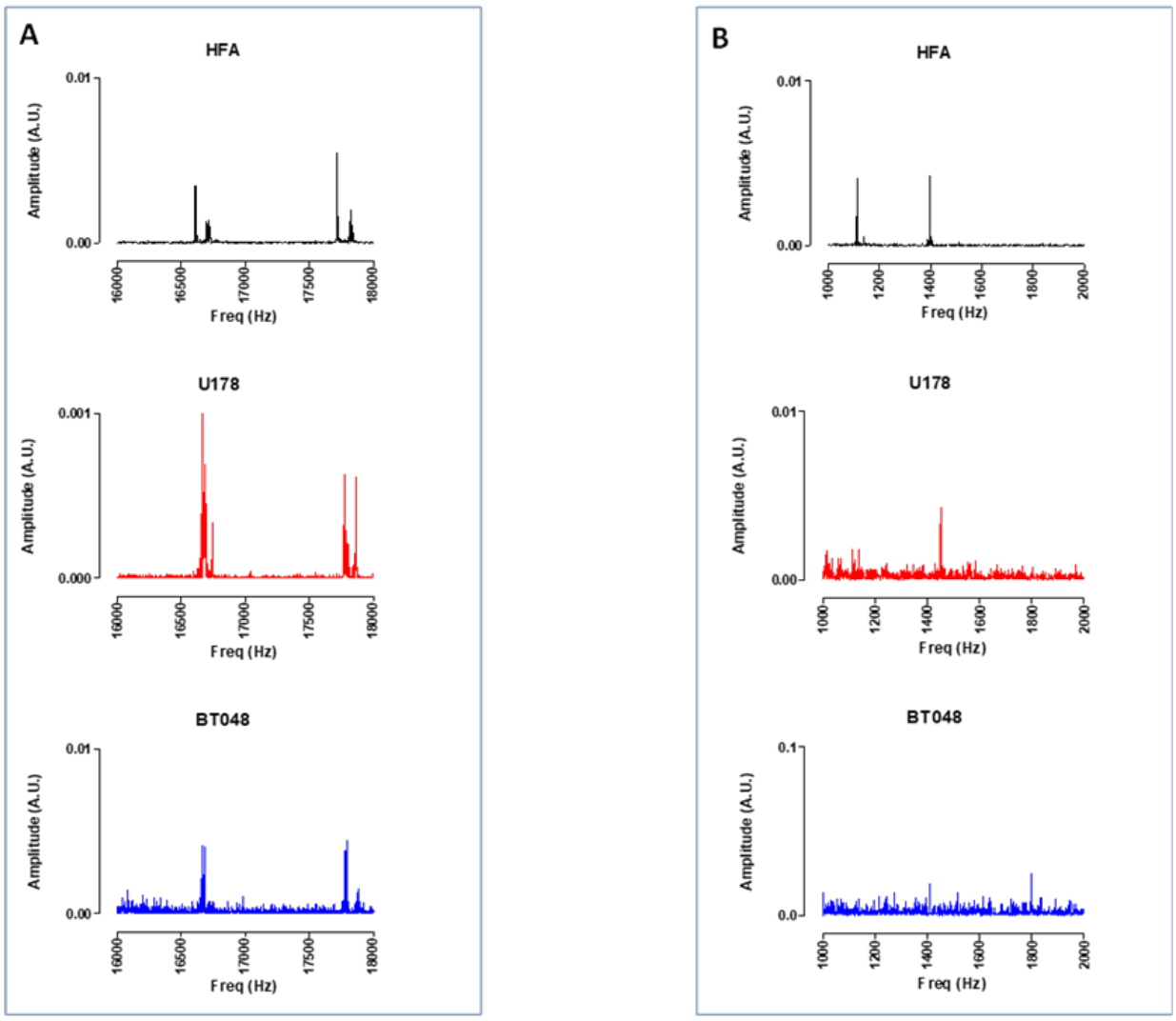

Figure 3.5: Spectral comparison of astrocytes and glioma cancer cells. Panel A depicts a sample of the major frequency peak present in all the cell types. A doublet frequency peaks between the range of 16.5 – 17 KHz and 17.5 – 18 KHz. Panel B shows differences in spectral comparison. Two peaks were present at 1050 and 1400 Hz in HFA cells, 1450 Hz in U178 Hz, but no frequency peaks were observed in BT048 cells in this range. FFT powers are represented as normalized arbitrary units (A.U.).

3.3.3 Vibration recording from brain tumors and neocortex

Metabolic activity of brain tumors can indicate the aggressiveness of a patient's tumor and is important for making treatment decisions (67,68). Therefore, vibrational profiling may have a potential application for patient care, particularly given that metabolic information can be obtained in real-time using this approach. In view of our results demonstrating a correlation between basal RMS and metabolism in untreated tumor cell cultures, we next obtained fresh brain tumor samples from surgical resections and recorded their vibrational profiles. To evaluate the method, we compared force vibration signals between three malignant astrocytoma specimens to three meningiomas. Tissues from the lateral temporal neocortex, taken during the removal of epileptic foci sites from two patients, were used for control. Patient information is detailed in Methods and Procedures, Section 3.2.4, Table 1. As expected, the RMS of fluctuations was significantly greater for the malignant astrocytoma specimens, which are known to be highly metabolically active (Fig. 4.2D). Interestingly, RMS values were similar for samples taken from patients with meningiomas and tissues from control patients, but both were markedly different from samples from malignant astrocytomas (Fig. 4.2A-C). The latter showed greater vibrational heterogeneity, perhaps reflective of the morphologic heterogenity of malignant astrocytomas. It is also possible that focal areas of necrosis, often present in high-grade tumors, could have influenced the findings. Larger patient samples and direct correlation with pathology will be required to answer these questions. Nonetheless, it is exciting to speculate that RMS may be a useful technique for phenotyping gliomas and for measuring brain tumor metabolism in real-time.

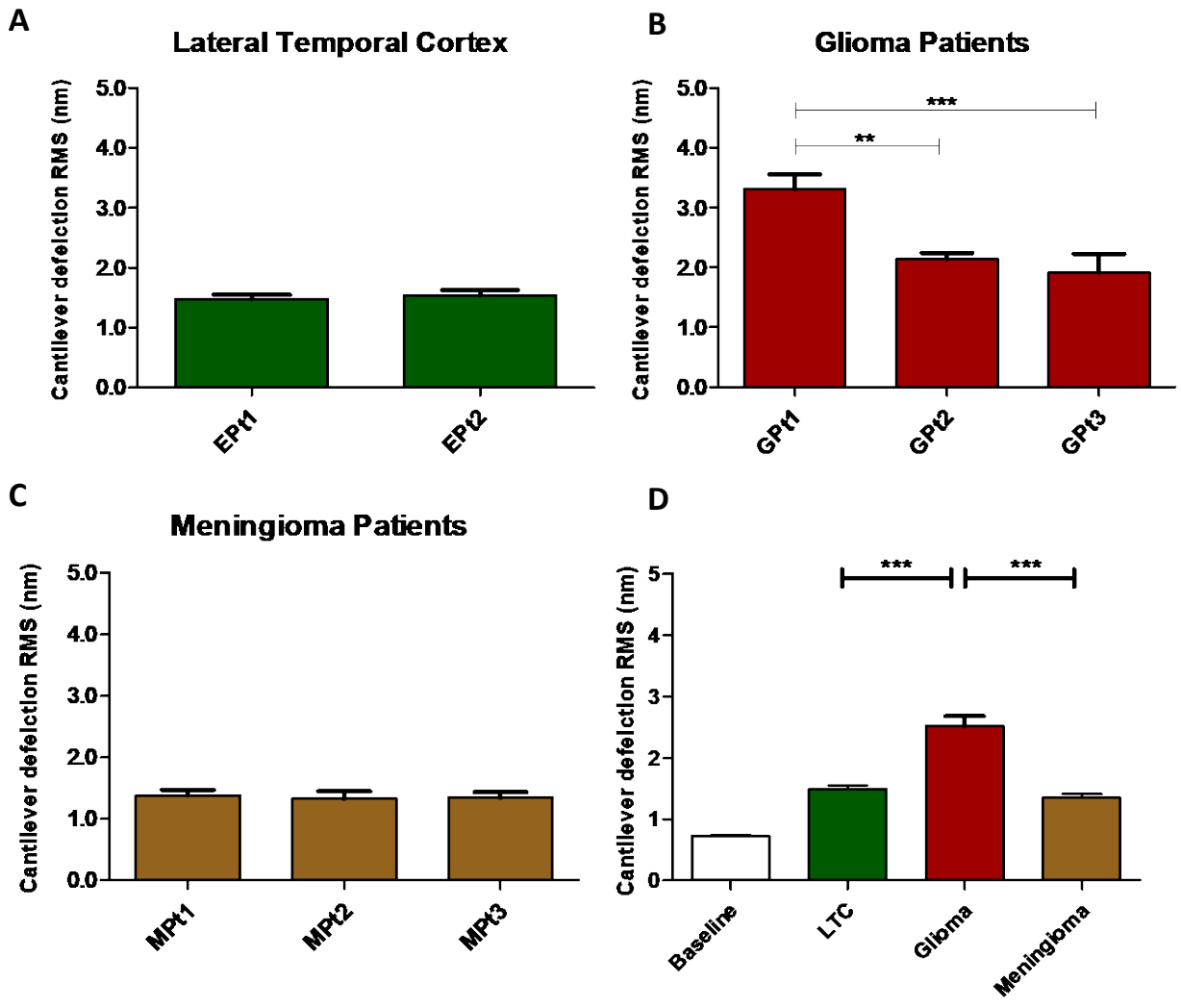

Figure 3.6: Time domain RMS analysis of brain tumor patients. Quantified RMS values according to patient (Pt) and brain types are depicted in (A) LTC (Lateral temporal cortex), (B) glioma (malignant astrocytoma) and (C) meningioma for each patient studied. (D) Average deflection RMS for all human LTC, malignant astrocytoma and meningioma tissues obtained from the operating room is compared to baseline RMS recordings. Bars in deflection plots represent mean RMS values ± SEM.

3.3.4 Vibrational spectral characterization of brain tumors and neocortex

We next performed spectral analyses of the brain tumor and cortex tissue vibrations. Meningioma spectra showed a narrow cluster of peaks at 4.23±1.65 Hz (n = 3 patients), while malignant astrocytoma showed a group of peaks at 3.65±0.29, 11.01±0.51, 18.48±0.76, 28.29±1.38 and 36.30±0.28 Hz, (n=3 patients). A distinct cluster of peaks at 3.38±0.29 Hz (n=2 patients) was ascribed to lateral temporal cortex (Figure 3.6A-C, top panels). The frequency peak ranges for meningioma and lateral temporal cortex overlapped. However, meningioma demonstrated a much broader peak cluster compared to the lateral temporal cortex, allowing differentiation between these two signals. The bands of these frequency clusters are depicted in normal probability plots (Figure 3.7). To detect dominant frequency peaks and reduce the background noise, we calculated Welch's Power Spectral Density function of each force signal (Figure 3.6A-C, middle panels). Scatter plots of dominant frequency peaks extracted from Welch's plots for each of the tissue specimens are depicted in Figure 3.6A-C, bottom panels. Most importantly, each spectrum profile was consistent between patients with the same class of tumor, which confirmed tumors demonstrate a unique signature frequency pattern that discriminates brain tumors by type, and from lateral temporal cortex tissue.

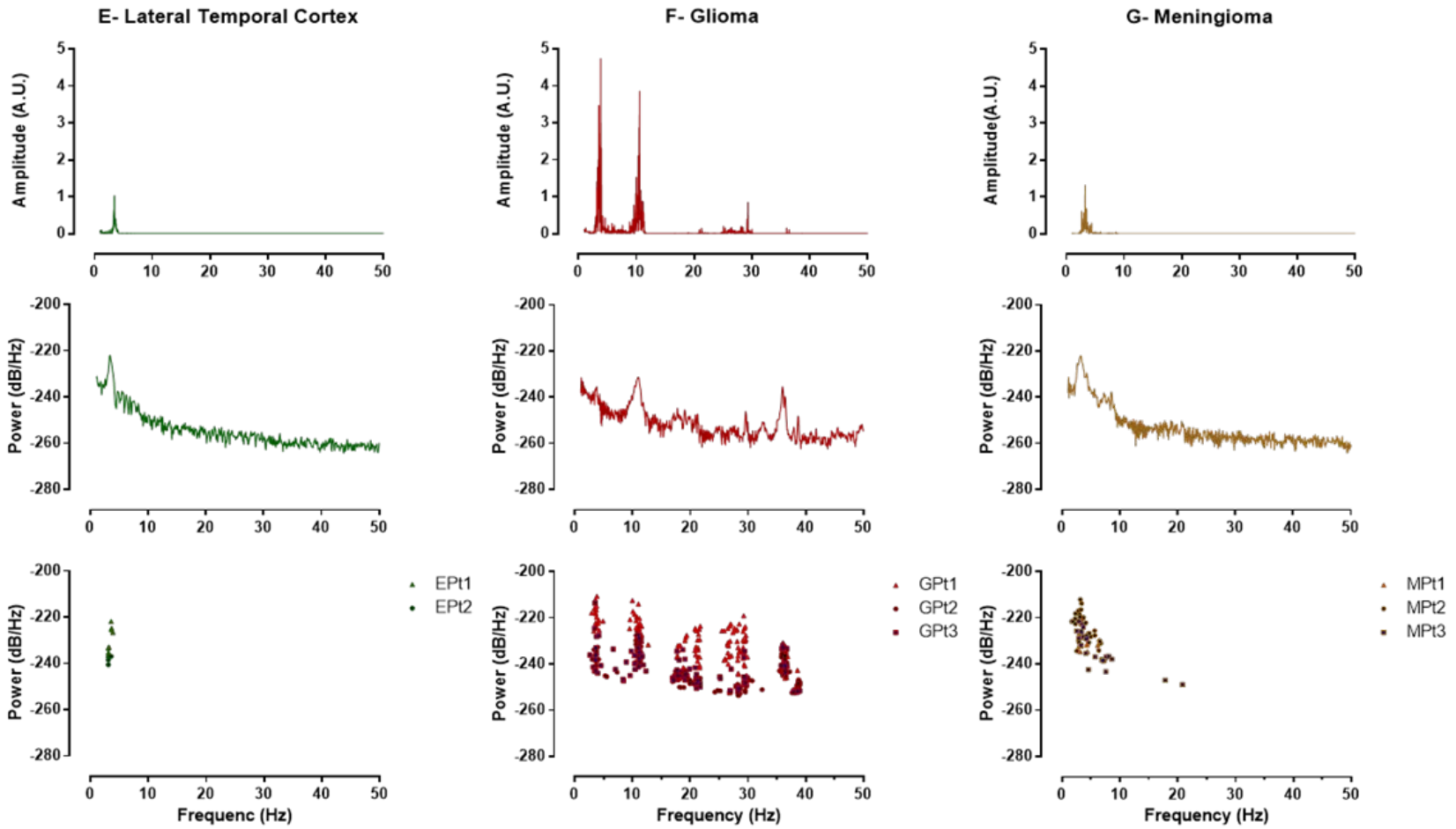
E- Lateral Temporal Cortex
F- Glioma
G- Meningioma
Amplitude (A.U.)
Amplitude(A.U.)
Power (dB/Hz)
Frequenc (Hz)
Frequency (Hz)
EPt1
EPt2
GPt1
GPt2
GPt3
MPt1
MPt2
MPt3

Figure 3.7: Spectral analysis of brain tumor patients. (A-C) Top panels: Representative FFT plots of force vibrations of LTC, malignant astrocytoma and meningioma. Middle panels: Representative Welch's power spectral density of LTC, malignant astrocytoma and meningioma. Lower panels: Scatter plots of dominant frequency peaks from all patient samples of LTC, malignant astrocytoma and meningioma demonstrating consistent spectral results between patients. FFT powers are represented as arbitrary units (A.U.).

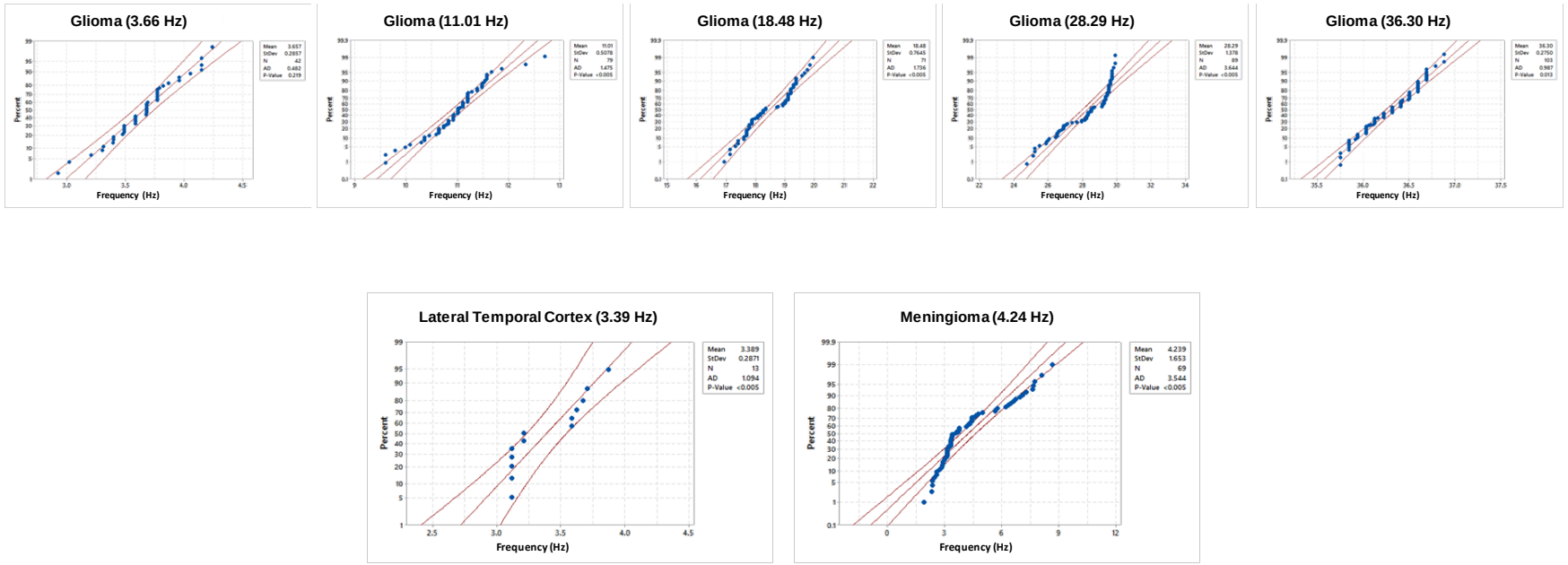

Figure 3.8: Normal probability plots of frequency clusters calculated with Welch's analysis of malignant astrocytoma (3.65, 11.01, 18.48, 28.29 & 36.30 Hz), lateral temporal cortex (3.38 Hz) and meningioma: (4.23 Hz). Welch plots are depicted in Fig. 3.6A-C, bottom panels

3.3.5 Acoustic profiling of brain tumors and neocortex

Characterizing cancers by vibration signature could prove to be an extremely important tool in cancer diagnostics. However, simplifying steps to interpret vibrational spectra results would be necessary for clinical translation of this novel observation. Therefore, we next applied demodulation techniques to convert recorded tissue vibration signals into audible sound (Supplementary Wave Files: 1-Malignant Glioma, 2-Meningioma and 3-Lateral Temporal Cortex). Since the distinguishing frequency clusters for each of the tumor and cortical tissues were below the audible range, the signals were modulated with an audio frequency-shift keying method (shifting the pitch), at baseband frequencies within the hearing range (69). This technique alters the pitch of a digital audio signal, so the listener can distinguish unique sounds, without a high-quality speaker. To avoid clipping, signals were normalized prior to the modulations. This work describes one plausible way that complex vibrational spectral analysis of tumors can be translated into a medium that medical specialists, such as surgeons, pathologists and technicians, can use to easily interpret and differentiate cancerous tumors from healthy brain tissues.

3.4 Discussion and conclusion

The few reports that have used contact-free AFM to measure membrane fluctuations in single cultured cells have implied that amplitude of fluctuations might correlate to cellular metabolism (5,16,39). Studying metabolism is vastly important in cancer research, as cancerous cells maintain a state of high metabolic output in order to sustain uncontrolled cell proliferation and aid in understanding how these mechanisms might offer new ways of treating cancers (62). Accordingly, we examined the clinical potential of an AFM's contact-free mode to detect nanoscale vibrations by testing its effectiveness to differentiate cancer cell lines. For any of the three cultured cell lines, U178 aggressive glioma type, BT048 slow-growing tumor, and HFA common control, Fast Fourier Transform (FFTs) analysis did not reveal any major frequency peaks. However, fast-growing U178 cells exhibited significantly higher RMS as compared to the slow-growing BT048, and HFA cells (Fig. 3.2D). Similar to previous studies, referenced above, this method is unable to determine whether fluctuation changes were a reflection of overall metabolism changes, or solely the result of inhibiting specific cellular components targeted by a drug. This prompted us to perform bioenergetic experiments on cancerous cell lines, in culture, to reveal whether the oxygen consumption rates of untreated cells, at basal resting conditions, resembled RMS levels in untreated cells.

Indeed, this was the case. RMS values for cell lines resembled the pattern of the basal oxygen consumption rate. Importantly, we observed little variance in RMS between samples of the same cell-type, which demonstrated our ability to reproduce the technique across multiple preparations of cell cultures. A direct correlation between cell metabolism and vibration will require testing additional cell lines and examining the actions of additional metabolic inhibitors on

RMS. This was outside the scope of our preliminary work. We speculate on the potential of contact-free AFM to determine the mitochondrial respiration of cancer cells in culture with different growth rates. Future investigations in this area will be of interest in evaluating the utility of this method to gauge the aggressiveness of cancer, and/or to monitor patient responses to cancer therapy.

Mechanical vibrations appear to be a ubiquitous signature of life, which may be linked to overall cellular activity. However, the potential information content of a spectrum is correlated to its ability to reveal the spectral content. In this respect, AFM methods appear to be less promising, with few main spectral components that appeared within a limited bandwidth of 1 Hz to about 30 Hz at the tissue level. The contact-free AFM method was limited in its capacity to resolve frequency spectra due to the inherent mechanical property of the cantilevers used as vibration probes. We attribute the lack of spectral profile in cultured cells to the AFM probe (cantilever) stiffness and its susceptibility to thermal fluctuations, which may have dampened and hindered the vibration patterns to be resolved. Moreover, in the AFM technique the frequency bandwidth of spectral analysis was limited to the first resonance frequency, which is typically 1-3 kHz. To see if samples produce more detail-rich spectra that were not resolved in the AFM, we switched to the more sensitive optical tweezers (OT). Individual cells were held suspended in the focal spot of a laser and their fluctuations detected directly. In addition to reproducing the AFM RMS results, FFT spectral analysis showed many prominent peaks up to about 50 kHz, creating a detailed spectral fingerprint for each cell type examined.

Our results clearly suggest OT greatly exceeds the sensitivity and bandwidth of the traditional AFM setup for vibrational profiling and should be used whenever possible. However,

the inherent limitation to the OT detection system is that opaque tissue specimens, such as brain tissue, need to be studied in the AFM contact-free method.

Our preliminary RMS data from tumor and cortical tissue specimens indicated RMS is a reliable way to measure tumor metabolism. (70,71). Although we acknowledge future work must be done to confirm RMS is indicative of metabolism at the tissue level, it is exciting to envision the potential use of this technology, not only for information on tumor type based on distinctive vibrational frequency patterns, but also that it may indicate the metabolic state of a tumor.

Importantly, it was the additional frequency spectra analysis conducted on recorded fluctuations that separated this technique from preceding AFM methods. We were able to identify tumor cells and tissues, even in the presence of highly heterogeneous cancer tissue regions. Vibrational analysis makes it possible to isolate specific frequency patterns that are unique to specific biological processes and tissue types. This was particularly important for identifying meningioma from healthy tissue; which could not be distinguished solely by amplitude of fluctuations (RMS). Irrespective of RMS readings, each brain tumor and cortical specimen displayed a remarkably consistent frequency peak signature. Given we have shown a method to convert these vibrational signatures into sound, if this technology were translated to the operating room, a surgeon might use this feature in the form of a scanning probe, allowing the removal of tumor tissue until the sound profile of cancerous tissue was no longer apparent. While clinical translation of this concept would allow a surgeon to interrogate tissue during surgery, it is not feasible using current technology. Devising a self-sensing piezoresistive cantilever assembled on a chip holder at the end effector of a medical robot may be possible. Such a device would not only

record nanoscale tissue vibrations, but also resolve problems associated with potential laser hazards and an unwieldy AFM setup.

To use the AFM system in its present form to detect which cells are cancerous and which ones are not would require setting up the microscope in a space adjacent to the operating room. This could provide the surgeon with diagnostic information on the tissue within ~10 minutes, which could be a major improvement to current neurosurgical intraoperative consultation turnaround times for histopathology, which currently range from 30-60 minutes. However, histology reports for brain tumors conducted in this timeframe are often inconclusive and provide only a qualitative assessment, whereas vibration profiling is a quantitative measurement that effectively identifies tissue type.

In conclusion, the results presented in this chapter demonstrate the potential use of AFM and OT in the detection of the alterations that occur in cells and tissues when they transform from normal to a diseased state. Thus, the results show the ability of vibrational profiling to be used as alternative method in cancer detection research.

Chapter Four: **Final discussion and conclusion**

4.1 Restatement of objective

The study of cellular activity and membrane fluctuation through nano-mechanical oscillation is an emerging field, with previous measurement of cell vibration restricted to single cells. Single prokaryotic and eukaryotic cells were shown, using the cantilever of an atomic force microscope (AFM) to mechanically oscillate (5,7,39). The magnitude of these nanoscale fluctuations was shown to have a direct link to a cell's metabolic activity. Furthermore, it was found that the vibration detected can be modulated using pharmacological agents such as metabolic blockers and chemotherapy, suggesting that nanomechanical vibration is a common feature of living cells.(5).

In this dissertation, we investigated the phenomenon observed for single cells to determine if it could be used to detect vibrational signatures in cultured cells, and at the tissue level. Given the brain is one of the most metabolically-active regions of the body, and our underlying interest in the future application of this methodology for potential brain tumor identification, we investigated the application of cellular vibration in neuronal cells and tissues.

4.2 Methods used to detect nano-mechanical vibration from biological samples

The complete AFM and OT experimental setups used in our study are detailed in Figure 2.1 and 3.1. Briefly, we custom-developed AFM and OT based methods to detect cellular vibration without direct physical contact with the samples. The systems were housed in a custom-assembled isolation chamber maintained at a constant temperature and 5% CO_2/ atmospheric O_2 levels. Barriers were used to minimize and account for external sources of vibration. For offline vibration signal analysis, we also utilized customized MATLAB algorithms (Appendix B)**.** Both the AFM

and OT were connected to a spectrum analyzer to demonstrate the potentials of intuitive and real-time assessment capability of both methods.

4.3 Key findings in *ex-vivo* animal model testing

Our results from animal models suggest vibrational profiling may prove to be a useful technique in studying healthy brain function and neural networks. In the rat brain, neuronal firing rates differed substantially between brain regions and maturity. In newborn rats, the hippocampus was intrinsically more active than the cerebellum due to the limited neuronal architecture at this time point in the development of the cerebellum, whereas some of the pyramidal cell circuitry in the hippocampus was established (72-75). Indeed, in both hippocampal cultures and tissue, a major frequency peak was present but none was identified in cerebellar sample, unless chemically depolarized. From these experiments, we concluded that for the studied brain tissues, a large portion of the detected cellular vibration was due to neuronal activity; this was also true for the major peak observed at ~3.4 Hz. In support of this assumption, the major frequency peak at ~3.4 Hz we observed in resting state hippocampal tissue correlates to reported electrophysiology-detected spontaneous and synchronous 3.4 Hz theta rhythm firing rates of pyramidal neurons in rat hippocampus and prefrontal cortex *in-vivo* during working memory task (76,77). However, the precise mechanism of how neuronal activity propagates nanoscale oscillations, or the contribution of other cellular processes -- for example, synaptic activity -- remains to be resolved. Furthermore, it will be important to understand how synchronous vibrations are governed and modulated, for example, in the developing and adult brain (78,79). Another intriguing question that extends beyond the scope of this study concerns the biological importance of specific vibration patterns in the brain. Is synchronized vibration part of a cellular pacemaking mechanism (80)? Do these synchronized oscillations factor in shaping brain function as in, for instance, input frequency

specific plasticity observed in the central auditory nervous system? (81) If this is the case, could cellular vibration in the brain influence biological processes in a way similar to how transcranial focused ultrasound (82) and magnetic brain stimulations (83) are used in clinical intervention and can modulate cortical function in humans? Furthermore, can we use the observed nano-mechanical vibration patterns similar to electroencephalography (EEG), and are vibration signatures characteristic of specific diseases (84)?

Irrespective of the mechanism used to excite the vibration source, the unique observation we present of an animal model demonstrates a novel procedure to simultaneously record metabolic activity and neuronal activity in a way that is not yet possible with any single existing technology. The findings presented here are vital to the study and understanding of the close relationship between neuronal activity and cell metabolism in single cells. Additionally, we have presented a way to map this metabolic activity in the brain using the contact-free AFM method we developed. Furthermore, we can use this technique to record the biological activity of cells without direct physical interaction, allowing the study of cells in their natural state. This offers an advantage over current techniques -- such as, electrophysiology -- that require direct interaction with the cell membranes, and risk possible damage to the cells.

4.4 Clinical application: vibration profiling of brain tumor cells and tissues.

We also investigated the clinical potential of the contact-free AFM method by assessing its effectiveness to identify tumor cells and tumor tissues removed from donor patients. In this respect, we first assessed the relationship between the intensity of fluctuation measured in RMS and metabolism. Studying metabolism is of the utmost importance in cancer research, as cancerous cells maintain a state of high metabolic output in order to sustain uncontrolled cell proliferation.

It is also important to understand how the metabolic rate of cells and tissues might offer ways of treating cancers (62). Accordingly, drugs that target metabolic pathways by stopping energy synthesis are known to be very effective chemotherapeutic agents. Tumor metabolic activity is also a reflection of a tumor's aggressiveness and can be used as a prognostic predictor. Furthermore, measuring metabolic rate is an important method to identify tumors in the body through imaging techniques that include fluorodeoxyglucose positron emission tomography (FDG-PET) (85-87).

In regard to establishing this potential, clinically-relevant link, previous AFM-based studies, that monitored cantilever deflection changes following the treatment of cells with drugs known to interfere with cellular metabolism, have presented preliminary data that links metabolism to nanoscale membrane fluctuations (5,16). Indeed, we observed similar results, i.e. RMS was significantly reduced in neuronal cultures treated with the mitochondrial inhibitor, sodium azide. However, no direct measurement of the metabolic state was carried out in previous investigations, making it difficult to confirm from these studies whether changes in fluctuations were a reflection of overall metabolism, or solely the result of inhibiting specific cellular components targeted by the drug. This prompted us to obtain more evidence to establish a link between metabolism and cellular fluctuations. Accordingly, we performed bioenergetics experiments on cancerous cell lines in culture and found that oxygen consumption rates of untreated cells at resting conditions correlated to RMS. Importantly, little variance in RMS was observed between samples of the same cell-type. We envisage cellular vibration profiling (VP) could be an important tool for studying metabolism in the culture models of cancer cells, e.g. monitoring RMS changes of cells in response to drug treatment.

The greatest potential of vibration profiling of biological samples lies in the information content of spectral analysis. In this respect, AFM methods were not promising, with few main spectral components that appeared within a limited bandwidth of 1 Hz to about 30 Hz. The contact-free AFM method was limited in its capacity to resolve frequency spectra due to the inherent mechanical property of cantilevers used as vibration probes. Therefore, we developed a more force sensitive vibration detection method using optical tweezers (OT) for single cell vibration profiling. Analysis of OT results showed the capability to reproduce RMS trends observed in the AFM technique, and more importantly, we observed detail rich spectral fingerprinting resolved prominent peaks appearing up to 50 KHz.

Understanding these spectral rich fingerprint signals in full, including the underlying biological processes that cause them, and how to take advantage of this knowledge to address biological problems, is beyond the scope of this project, and should be investigated further as a future direction of this project. However, at this point, we speculate that the vibrational signatures observed from single cells in OT could be a reflection of a substantive subset of all active and dynamic processes of cells at the time of recording. This collective of cellular processes defines to a large degree a phenotype of the cells studied. The dynamic cellular processes may occur at a specific (catalytic) rate, leading directly to a spectral peak observed, and contributing to the RMS of the signal. Therefore, we concluded mechanical vibrations appear to be a ubiquitous signature of life, which may be linked to overall cellular activity.

The sensitivity of OT force detection is superior to the AFM technology. However, the OT's vibration detection is restricted by the tissue's degree of transparency, therefore, the AFM setup should be used for opaque tissues like the brain. Alternatively, further investigation is

required if current obstacles regarding tissue interrogations by OT can be overcome. In this case, we propose the laser light of OT could be used to trap tissue structures, such as the nucleus or mitochondria inside the tissue that then act as a probe, akin to the mass of an accelerometer. Alternatively, one could potentially insert nano-particles into the tissue to act as sensors to overcome the technical limitations of the OT used to study tissues. In the meantime, the contact-free AFM method is best suited to study tissue biopsies.

In Chapter 3, we also assessed the practical, clinically-relevant application of the AFM to differentiate brain tumours (malignant astrocytoma, meningioma) from normal brain tissue (lateral temporal cortex (LTC)) on the basis of vibration signatures. The results showed a capacity to differentiate malignant astrocytoma from meningioma or lateral temporal cortex based on RMS and frequency domain patterns. Our preliminary RMS data from tumor and cortical tissue specimens certainly points towards RMS as being a reliable measure of tumor metabolism; results followed the metabolism trends of tumor types tested in other conventional methods (70,71). Although we do acknowledge future work must be done to confirm RMS is indicative of metabolism at the tissue level, it is exciting to envision use of this technology not only to indicate the metabolic state of a tumor, but it provides information on tumor type based on unique vibration frequency patterns.

Most importantly, it was the additional frequency spectra analysis conducted on recorded fluctuations which allowed us to better discriminate tumors and tissues with high reproducibility and accuracy, even in the presence of highly heterogeneous tissue regions. The distinctive feature of vibrational analysis makes it possible to isolate from overall fluctuation recordings, specific frequency clusters unique to specific biological processes or tissue types. This turned out to be

particularly important for identifying meningioma from healthy tissue, which could not be distinguished by amplitude of fluctuations (RMS) alone. Irrespective of RMS readings, each brain tumor and cortical specimen displayed a remarkably consistent frequency peak signature. Furthermore, we have shown a method to convert the vibration signals to sound files to allow for a novel acoustic technique to identify abnormal tissue. If translated in a clinical setting -- or more specifically, to the operating room -- it could provide a third dimension of *sound*, in addition to *vision* and *touch* to differentiate abnormal from normal tissue during surgery.

References

(1) Strey H, Peterson M, Sackmann E. Measurement of erythrocyte membrane elasticity by flicker eigenmode decomposition. Biophys J 1995;69(2):478-488.

(2) Levin S, Korenstein R. Membrane fluctuations in erythrocytes are linked to MgATP-dependent dynamic assembly of the membrane skeleton. Biophys J 1991;60(3):733-737.

(3) Mittelman L, Levin S, Korenstein R. Fast cell membrane displacements in B lymphocytes Modulation by dihydrocytochalasin B and colchicine. FEBS Lett 1991;293(1-2):207-210.

(4) Krol AY, Grinfeldt M, Levin S, Smilgavichus A. Local mechanical oscillations of the cell surface within the range 0.2–30 Hz. European Biophysics Journal 1990;19(2):93-99.

(5) Kasas et al. Detecting nanoscale vibrations as signatures of life. Proc Natl Acad Sci U S A 2015;112(2):378.

(6) Pelling et al. Local Nanomechanical Motion of the Cell Wall of Saccharomyces cerevisiae Supporting Material. 2004.

(7) Pelling AE, Sehati S, Gralla EB, Gimzewski JK. Time dependence of the frequency and amplitude of the local nanomechanical motion of yeast. Nanomedicine: Nanotechnology, Biology and Medicine 2005;1(2):178-183.

(8) Wu S, Liu X, Zhou X, Liang XM, Gao D, Liu H, et al. Quantification of cell viability and rapid screening anti-cancer drug utilizing nanomechanical fluctuation. - Biosens Bioelectron.2015 Sep 14;77:164-173.doi: 10.1016/j.bios.2015.09.024. (1873-4235 (Electronic); 0956-5663 (Linking)).

(9) Sanai N, Berger MS. Glioma extent of resection and its impact on patient outcome. Neurosurgery 2008;62(4):753-766.

(10) Wen PY, Kesari S. Malignant gliomas in adults. N Engl J Med 2008;359(5):492-507.

(11) Sanai N, Mirzadeh Z, Berger MS. Functional outcome after language mapping for glioma resection. N Engl J Med 2008;358(1):18-27.

(12) Jermyn M, Mok K, Mercier J, Desroches J, Pichette J, Saint-Arnaud K, et al. Intraoperative brain cancer detection with Raman spectroscopy in humans. Sci Transl Med 2015 Feb 11;7(274):274ra19.

(13) Roelcke U. PET: Brain tumor biochemistry. J Neurooncol 1994;22(3):275-279.

(14) Peeling J, Sutherland G. High-Resolution 1H NMR spectroscopy studies of extracts of human cerebral neoplasms. Magnetic resonance in medicine 1992;24(1):123-136.

(15) Stummer W, Pichlmeier U, FAU - Meinel T, Meinel T, FAU - Wiestler OD, Wiestler OD, et al. Fluorescence-guided surgery with 5-aminolevulinic acid for resection of malignant glioma: a randomised controlled multicentre phase III trial. - Lancet Oncol.2006 May;7(5):392-401. (1470-2045 (Print); 1470-2045 (Linking)).

(16) Longo G, Alonso-Sarduy L, Rio LM, Bizzini A, Trampuz A, Notz J, et al. Rapid detection of bacterial resistance to antibiotics using AFM cantilevers as nanomechanical sensors. Nature nanotechnology 2013;8(7):522-526.

(17) Krol AY, Grinfeldt M, Levin S, Smilgavichus A. Local mechanical oscillations of the cell surface within the range 0.2–30 Hz. European Biophysics Journal 1990;19(2):93-99.

(18) Huang Q, Lee J, Arce FT, Yoon I, Angsantikul P, Liu J, et al. Nanofibre optic force transducers with sub-piconewton resolution via near-field plasmon–dielectric interactions. Nature Photonics 2017;11(6):352-355.

(19) El Hady A, Machta BB. Mechanical surface waves accompany action potential propagation. Nature communications 2015;6.

(20) Tuvia S, Levin S, Korenstein R. Correlation between local cell membrane displacements and filterability of human red blood cells. FEBS Lett 1992;304(1):32-36.

(21) Alster Y, Loewenstein A, Levin S, Lazar M, Korenstein R. Low-frequency submicron fluctuations of red blood cells in diabetic retinopathy. Arch Ophthalmol 1998;116(10):1321-1325.

(22) Verschueren H, Dekegel D, De Baetselier P. Difference in motile behavior between lymphoma variants with different invasive and metastatic capabilities. Invasion Metastasis 1988;8(1):31-44.

(23) Partin AW, Schoeniger JS, Mohler JL, Coffey DS. Fourier analysis of cell motility: correlation of motility with metastatic potential. Proc Natl Acad Sci U S A 1989 Feb;86(4):1254-1258.

(24) Mittelman L, Levin S, Korenstein R. Fast cell membrane displacements in B lymphocytes Modulation by dihydrocytochalasin B and colchicine. FEBS Lett 1991;293(1-2):207-210.

(25) Vertessy BG, Steck TL. Elasticity of the human red cell membrane skeleton. Effects of temperature and denaturants. Biophys J 1989;55(2):255-262.

(26) Mittelman L, Levin S, Verschueren H, Debaetselier P, Korenstein R. Direct correlation between cell membrane fluctuations, cell filterability and the metastatic potential of lymphoid cell lines. Biochem Biophys Res Commun 1994;203(2):899-906.

(27) Verschueren H, Dekegel D, De Baetselier P. Difference in motile behavior between lymphoma variants with different invasive and metastatic capabilities. Invasion Metastasis 1988;8(1):31-44.

(28) Alonso-Sarduy L, De Los Rios P, Benedetti F, Vobornik D, Dietler G, Kasas S, et al. Real-time monitoring of protein conformational changes using a nano-mechanical sensor. PloS one 2014;9(7):e103674.

(29) Mahaffy R, Park S, Gerde E, Käs J, Shih C. Quantitative analysis of the viscoelastic properties of thin regions of fibroblasts using atomic force microscopy. Biophys J 2004;86(3):1777-1793.

(30) Radmacher M. Studying the mechanics of cellular processes by atomic force microscopy. Methods Cell Biol 2007;83:347-372.

(31) Muller DJ, Dufrene YF. Atomic force microscopy: a nanoscopic window on the cell surface. - Trends Cell Biol.2011 Aug;21(8):461-9.doi: 10.1016/j.tcb.2011.04.008.Epub 2011 Jun 12. (1879-3088 (Electronic); 0962-8924 (Linking)).

(32) Nievergelt AP, Erickson BW, Hosseini N, Adams JD, Fantner GE. Studying biological membranes with extended range high-speed atomic force microscopy. Scientific reports 2015;5.

(33) Amrein M, Shi Y. Method and apparatus for determining the cell activation of a target cell by an activator 2015.

(34) Lal R, Ramachandran S, Arnsdorf MF. Multidimensional atomic force microscopy: a versatile novel technology for nanopharmacology research. The AAPS journal 2010;12(4):716-728.

(35) Ivenshitz M, Segal M. Neuronal density determines network connectivity and spontaneous activity in cultured hippocampus. J Neurophysiol 2010 Aug;104(2):1052-1060.

(36) Opitz T, De Lima AD, Voigt T. Spontaneous development of synchronous oscillatory activity during maturation of cortical networks in vitro. J Neurophysiol 2002 Nov;88(5):2196-2206.

(37) Lahtinen H, Palva JM, Sumanen S, Voipio J, Kaila K, Taira T. Postnatal development of rat hippocampal gamma rhythm in vivo. J Neurophysiol 2002 Sep;88(3):1469-1474.

(38) Behroozi F. Fluid viscosity and the attenuation of surface waves: a derivation based on conservation of energy. European journal of physics 2003;25(1):115.

(39) Pelling AE, Sehati S, Gralla EB, Valentine JS, Gimzewski JK. Local nanomechanical motion of the cell wall of Saccharomyces cerevisiae. Science 2004 Aug 20;305(5687):1147-1150.

(40) McKay BE, Turner RW. Physiological and morphological development of the rat cerebellar Purkinje cell. J Physiol (Lond) 2005;567(3):829-850.

(41) Milner T, Loy R, Amaral D. An anatomical study of the development of the septo-hippocampal projection in the rat. Dev Brain Res 1983;8(2):343-371.

(42) Altman J. Postnatal development of the cerebellar cortex in the rat. II. Phases in the maturation of Purkinje cells and of the molecular layer. J Comp Neurol 1972;145(4):399-463.

(43) Altman J. Postnatal development of the cerebellar cortex in the rat. III. Maturation of the components of the granular layer. J Comp Neurol 1972;145(4):465-513.

(44) Leinekugel X, Medina I, Khalilov I, Ben-Ari Y, Khazipov R. Ca 2 oscillations mediated by the synergistic excitatory actions of GABA A and NMDA receptors in the neonatal hippocampus. Neuron 1997;18(2):243-255.

(45) Garaschuk O, Linn J, Eilers J, Konnerth A. Large-scale oscillatory calcium waves in the immature cortex. Nat Neurosci 2000;3(5):452-459.

(46) Crépel V, Aronov D, Jorquera I, Represa A, Ben-Ari Y, Cossart R. A parturition-associated nonsynaptic coherent activity pattern in the developing hippocampus. Neuron 2007;54(1):105-120.

(47) Karlsson KA, Blumberg MS. Hippocampal theta in the newborn rat is revealed under conditions that promote REM sleep. J Neurosci 2003 Feb 15;23(4):1114-1118.

(48) Blenkinsop TA, Lang EJ. Block of inferior olive gap junctional coupling decreases Purkinje cell complex spike synchrony and rhythmicity. J Neurosci 2006 Feb 8;26(6):1739-1748.

(49) Person AL, Raman IM. Synchrony and neural coding in cerebellar circuits. Frontiers in neural circuits 2012;6:97.

(50) Raichle ME, Mintun MA. Brain work and brain imaging. Annu Rev Neurosci 2006;29:449-476.

(51) Kaibara T, Saunders JK, Sutherland GR. Advances in mobile intraoperative magnetic resonance imaging. Neurosurgery 2000;47(1):131-138.

(52) In silico tumor growth: application to glioblastomas. International Conference on Medical Image Computing and Computer-Assisted Intervention: Springer; 2004.

(53) Coughlin MF, Bielenberg DR, Lenormand G, Marinkovic M, Waghorne CG, Zetter BR, et al. Cytoskeletal stiffness, friction, and fluidity of cancer cell lines with different metastatic potential. Clin Exp Metastasis 2013;30(3):237-250.

(54) Guck J, Schinkinger S, Lincoln B, Wottawah F, Ebert S, Romeyke M, et al. Optical deformability as an inherent cell marker for testing malignant transformation and metastatic competence. Biophys J 2005;88(5):3689-3698.

(55) Suresh S. Biomechanics and biophysics of cancer cells. Acta Materialia 2007;55(12):3989-4014.

(56) Cross S. Nanomechanical analysis of cells from cancer patients. Letters 2007;2:780-783.

(57) Cross SE, Jin Y, Tondre J, Wong R, Rao J, Gimzewski JK. AFM-based analysis of human metastatic cancer cells. Nanotechnology 2008;19(38):384003.

(58) Bailey RG, Turner RD, Mullin N, Clarke N, Foster SJ, Hobbs JK. The interplay between cell wall mechanical properties and the cell cycle in Staphylococcus aureus. Biophys J 2014;107(11):2538-2545.

(59) Fisher R, Pusztai L, Swanton C. Cancer heterogeneity: implications for targeted therapeutics. Br J Cancer 2013;108(3):479-485.

(60) Kuznetsova TG, Starodubtseva MN, Yegorenkov NI, Chizhik SA, Zhdanov RI. Atomic force microscopy probing of cell elasticity. Micron 2007;38(8):824-833.

(61) Longo G, Alonso-Sarduy L, FAU - Rio LM, Rio LM, FAU - Bizzini A, Bizzini A, et al. Rapid detection of bacterial resistance to antibiotics using AFM cantilevers as nanomechanical sensors. - Nat Nanotechnol.2013 Jul;8(7):522-6.doi: 10.1038/nnano.2013.120.Epub 2013 Jun 30. (1748-3395 (Electronic); 1748-3387 (Linking)).

(62) Cairns RA, Harris IS, Mak TW. Regulation of cancer cell metabolism. Nature Reviews Cancer 2011;11(2):85-95.

(63) Zhou Y, Larsen PH, Hao C, Yong VW. CXCR4 is a major chemokine receptor on glioma cells and mediates their survival. J Biol Chem 2002 Dec 20;277(51):49481-49487.

(64) Sarkar S, Nuttall RK, Liu S, Edwards DR, Yong VW. Tenascin-C stimulates glioma cell invasion through matrix metalloproteinase-12. Cancer Res 2006 Dec 15;66(24):11771-11780.

(65) Lawrence DM, Seth P, Durham L, Diaz F, Boursiquot R, Ransohoff RM, et al. Astrocyte differentiation selectively upregulates CCL2/monocyte chemoattractant protein-1 in cultured human brain-derived progenitor cells. Glia 2006;53(1):81-91.

(66) Sarkar S, Döring A, Zemp FJ, Silva C, Lun X, Wang X, et al. Therapeutic activation of macrophages and microglia to suppress brain tumor-initiating cells. Nat Neurosci 2014;17(1):46-55.

(67) Metabolic positron emission tomography imaging in cancer detection and therapy response. Seminars in oncology: Elsevier; 2011.

(68) Plathow C, Weber WA. Tumor cell metabolism imaging. J Nucl Med 2008 Jun;49 Suppl 2:43S-63S.

(69) Ghovanloo M, Najafi K. A wideband frequency-shift keying wireless link for inductively powered biomedical implants. Circuits and Systems I: Regular Papers, IEEE Transactions on 2004;51(12):2374-2383.

(70) Chen W. Clinical applications of PET in brain tumors. J Nucl Med 2007 Sep;48(9):1468-1481.

(71) Lee JW, Kang KW, Park S, Lee SM, Paeng JC, Chung J, et al. 18F-FDG PET in the assessment of tumor grade and prediction of tumor recurrence in intracranial meningioma. European journal of nuclear medicine and molecular imaging 2009;36(10):1574-1582.

(72) Miklowitz D.J., Otto M.W., Frank E., ReillyHarrington N.A., Kogan J.N., Sachs G.S., et al. Intensive psychosocial intervention enhances functioning in patients with bipolar depression: Results from a 9-month randomized controlled trial. Am J Psychiatry 2007 September 2007;164(9):1340-1347.

(73) Soares J.J.F., Macassa G., FandinoLosada A. Psychosocial experiences among female and male primary care patients with and without pain. Pain Clinic 2007 2007;19(2):58-70.

(74) Schene A.H., Koeter M.W.J., Kikkert M.J., Swinkels J.A., McCrone P. Adjuvant occupational therapy for work-related major depression works: Randomized trial including economic evaluation. Psychol Med 2007 March 2007;37(3):351-362.

(75) Schuler T.A., Kissane D.W., Zaider TI. Cluster analysis of perceived family functioning among an american sample of advanced cancer patients in the palliative care setting. Asia-Pacific Journal of Clinical Oncology 2012. November 2012;8:137-138.

(76) Fujisawa S, Buzsáki G. A 4 Hz oscillation adaptively synchronizes prefrontal, VTA, and hippocampal activities. Neuron 2011;72(1):153-165.

(77) Buzsaki G. Theta oscillations in the hippocampus. Neuron 2002 Jan 31;33(3):325-340.

(78) Trachtenberg JT, Chen BE, Knott GW, Feng G. Long-term in vivo imaging of experience-dependent synaptic plasticity in adult cortex. Nature 2002;420(6917):788.

(79) Holtmaat AJ, Trachtenberg JT, Wilbrecht L, Shepherd GM, Zhang X, Knott GW, et al. Transient and persistent dendritic spines in the neocortex in vivo. Neuron 2005;45(2):279-291.

(80) Ehsani S. Time in the cell: a plausible role for the plasma membrane. arXiv preprint arXiv:1210.0168 2012.

(81) Nelson SL, Kong L, Liu X, Yan J. Auditory cortex directs the input-specific remodeling of thalamus. Hear Res 2015;328:1-7.

(82) Legon W, Sato TF, Opitz A, Mueller J, Barbour A, Williams A, et al. Transcranial focused ultrasound modulates the activity of primary somatosensory cortex in humans. Nat Neurosci 2014;17(2):322.

(83) Lefaucheur J, André-Obadia N, Antal A, Ayache SS, Baeken C, Benninger DH, et al. Evidence-based guidelines on the therapeutic use of repetitive transcranial magnetic stimulation (rTMS). Clinical Neurophysiology 2014;125(11):2150-2206.

(84) Schnitzler A, Gross J. Normal and pathological oscillatory communication in the brain. Nature reviews.Neuroscience 2005;6(4):285.

(85) Gupta NC, Maloof J, Gunel E. Probability of malignancy in solitary pulmonary nodules using fluorine-18-FDG and PET. The Journal of Nuclear Medicine 1996;37(6):943.

(86) Padma M, Said S, Jacobs M, Hwang D, Dunigan K, Satter M, et al. Prediction of pathology and survival by FDG PET in gliomas. J Neurooncol 2003;64(3):227-237.

(87) Adams S, Baum RP, Stuckensen T, Bitter K, Hör G. Prospective comparison of 18 F-FDG PET with conventional imaging modalities (CT, MRI, US) in lymph node staging of head and neck cancer. European Journal of Nuclear Medicine and Molecular Imaging 1998;25(9):1255-1260.

(87) Adams S, Baum RP, Stuckensen T, Bitter K, Hör G. Prospective comparison of 18 F-FDG PET with conventional imaging modalities (CT, MRI, US) in lymph node staging of head and neck cancer. European Journal of Nuclear Medicine and Molecular Imaging 1998;25(9):1255-1260.

(88) Schwartzbaum JA, Fisher JL, Aldape KD, Wrensch M. Epidemiology and molecular pathology of glioma. Nature Reviews Neurology. 2006 Sep;2(9):494. 1

(89) Canadian Cancer Society. Brain and spinal cord tumors. http://www.cancer.ca/en/cancer-information/cancer-type/brain-spinal/diagnosis/?region=on. Updated 2016. Accessed 07/06, 2016. 2

(90) Sanai N, Berger MS. Glioma extent of resection and its impact on patient outcome. Neurosurgery. 2008 Apr 1;62(4):753-66. 3

(91) Wen PY, Kesari S. Malignant gliomas in adults. New England Journal of Medicine. 2008 Jul 31;359(5):492-507. 4

(92) Cameron RS, Rakic P. Glial cell lineage in the cerebral cortex: a review and synthesis. Glia. 1991 Jan 1;4(2):124-37. 5

(93) American brain tumor association. About brain tumors. http://www.abta.org/brain-tumor-information/. Updated 2016. Accessed 07/06, 2016. 6

(94) Schermelleh L, Heintzmann R, Leonhardt H. A guide to super-resolution fluorescence microscopy. The Journal of cell biology. 2010 Jul 26;190(2):165-75.

(95) Weilinger NL, Lohman AW, Rakai BD, Ma EM, Bialecki J, Maslieieva V, Rilea T, Bandet MV, Ikuta NT, Scott L, Colicos MA. Metabotropic NMDA receptor signaling couples Src family kinases to pannexin-1 during excitotoxicity. Nature neuroscience. 2016 Mar;19(3):432.

(96) Proctor DT, Stotz SC, Scott LO, de la Hoz CL, Poon KW, Stys PK, Colicos MA. Axo-glial communication through neurexin-neuroligin signaling regulates myelination and oligodendrocyte differentiation. Glia. 2015 Nov 1;63(11):2023-39.

(97) Stotz SC, Scott LO, Drummond-Main C, Avchalumov Y, Girotto F, Davidsen J, Gómez-Gárcia MR, Rho JM, Pavlov EV, Colicos MA. Inorganic polyphosphate regulates neuronal excitability through modulation of voltage-gated channels. Molecular brain. 2014 Dec;7(1):42.

(98) Colicos MA, Collins BE, Sailor MJ, Goda Y. Remodeling of synaptic actin induced by photoconductive stimulation. Cell. 2001 Nov 30;107(5):605-16.

(99) Gutierrez RC, Hung J, Zhang Y, Kertesz AC, Espina FJ, Colicos MA. Altered synchrony and connectivity in neuronal networks expressing an autism-related mutation of neuroligin 3. Neuroscience. 2009 Aug 4;162(1):208-21.

(100) Penn Y, Segal M, Moses E. Network synchronization in hippocampal neurons. Proceedings of the National Academy of Sciences. 2016 Mar 22;113(12):3341-6.

(101) Heidenreich RD. Fundamentals of transmission electron microscopy.

Appendix A – Sample sound wave attenuation calculation based Stoke theory.

$\eta = 1.10^{-3}$

$V = 1500$

$\rho = 998.2$

$\omega = 3$

$$\alpha = \frac{2.\eta.\omega^2}{3.\rho.V^3} \qquad 1.780983548\ 10^{-15}$$

$$d = 5.10^{-9} \qquad \frac{1}{200000000}$$

$e^{-\alpha.d}$ $\quad 1.$

$$d = 10.10^{-9} \qquad \frac{1}{100000000}$$

$e^{-\alpha.d}$ $\quad 1.$

$$d = 15.10^{-9} \qquad \frac{3}{200000000}$$

$e^{-\alpha.d}$ $\quad 1.$

$d = 0$ $\quad 0$

$e^{-\alpha.d}$ $\quad 1.$

Appendix B- Custom written MATLAB script for AFM raw data extraction

```
% Cell Vibration Analysis Script
% Developed by Sultan Nelson

% This custom written MATLAB script developed by Sultan Nelson

% INPUT
% Raw cell vibration digital data collected by AFM
% OUTPUT
% Time-time domain Plot
% Frequency-domain Plot
% Dominant Peak Scatter Plot
% Root Mean Square Plot

% DISCRIPTION
% The script first sorts data from multiple trials. It then it saves all the force fluctuations
% recorded from AFM and the segmental times in MATLAB's workspace.
% It filters out frequencies .001 to 1 HZ then plots three time domain fluctuations and three
frequency spectrum for each file opened.

% Version 1.5
% Updated December 2017
```

```
%-------------------------DATA IMPORT AND SORTING ------------------
% Import Data File 1 - 'Control'
[filename,path]=uigetfile('*.xlsx','Open Axon File');
data_1=xlsread(filename);
%Import Data File 2 - Live tissue or cell
[filename,path]=uigetfile('*.xlsx','Open Axon File');
data_2=xlsread(filename);
%Import Data File 3 - Tissue or cell after treatment
[filename,path]=uigetfile('*.xlsx','Open Axon File');
data_3=xlsread(filename);


%-----------------------------------------------------------------
% Raw Data sorting for file 1
k_1=find(~isnan(data_1(:,1)));
leng_1 =length(k_1);
d0_1=k_1(1);
m_1=1;
a1_1=1;
while k_1(m_1)==d0_1
    s0_1(a1_1)=k_1(m_1);
    m_1=m_1+1;
    d0_1=d0_1+1;
    a1_1=a1_1+1;
```

```
end
 d1_1=k_1(m_1);
a2_1=1;
while k_1(m_1)==d1_1
    s1_1(a2_1)=k_1(m_1);
    m_1=m_1+1;
    d1_1=d1_1+1;
    a2_1=a2_1+1;
end
 d2_1=k_1(m_1);
a3_1=1;
 while k_1(m_1)==d2_1
    s2_1(a3_1)=k_1(m_1);
    m_1=m_1+1;
    d2_1=d2_1+1;
    a3_1=a3_1+1;
end
 d3_1=k_1(m_1);
a4_1=1;
while k_1(m_1)==d3_1
    s3_1(a4_1)=k_1(m_1);
    m_1=m_1+1;
    d3_1=d3_1+1;
```

```
    a4_1=a4_1+1;
end
 d4_1=k_1(m_1);
a5_1=1;
while k_1(m_1)==d4_1
    s4_1(a5_1)=k_1(m_1);
    m_1=m_1+1;
    d4_1=d4_1+1;
    a5_1=a5_1+1;
end
 d5_1=k_1(m_1);
a6_1=1;
while k_1(m_1)==d5_1
    s5_1(a6_1)=k_1(m_1);
    m_1=m_1+1;
    d5_1=d5_1+1;
    a6_1=a6_1+1;
end
 d6_1=k_1(m_1);
a7_1=1;
while k_1(m_1)==d6_1
    s6_1(a7_1)=k_1(m_1);
    m_1=m_1+1;
```

```
    d6_1=d6_1+1;
    a7_1=a7_1+1;
end
 d7_1=k_1(m_1);
a8_1=1;
while k_1(m_1)==d7_1
    s7_1(a8_1)=k_1(m_1);
    m_1=m_1+1;
    d7_1=d7_1+1;
    a8_1=a8_1+1;
end
 d8_1=k_1(m_1);
a9_1=1;
while k_1(m_1)==d8_1
    s8_1(a9_1)=k_1(m_1);
    m_1=m_1+1;
    d8_1=d8_1+1;
    a9_1=a9_1+1;
end

d9_1=k_1(m_1);
a10_1=1;
while k_1(m_1)==d9_1
```

```
    s9_1(a10_1)=k_1(m_1);
    m_1=m_1+1;
    d9_1=d9_1+1;
    a10_1=a10_1+1;
end
 d10_1=k_1(m_1);
a11_1=1;
while k_1(m_1)==d10_1
    s10_1(a11_1)=k_1(m_1);
    m_1=m_1+1;
    d10_1=d10_1+1;
    a11_1=a11_1+1;
end
 d11_1=k_1(m_1);
a12_1=1;
while k_1(m_1)==d11_1
    s11_1(a12_1)=k_1(m_1);
    if m_1~=leng_1
    m_1=m_1+1;
    end
    d11_1=d11_1+1;
    a12_1=a12_1+1;
end
```

```
%-----------------------------------------------------------------------
% File 1 - Three out of twelve segments selected for analysis. "Touch"
% variable refers to the force fluctuation raw data. "Time" variable
% refers to the segmental time at which force fluctuation was recorded.
% Note: one file contains 6 total segments that can be used for analysis.
% In this case we have only selected to use 3 segments only.

%*** this segment is repeated for File 2 and File 3

touch1_1=data_1(s1_1,2);
time1_1= data_1(s1_1,6);
touch1_2=data_1(s5_1,2);
time1_2= data_1(s5_1,6);
touch1_3=data_1(s9_1,2);
time1_3= data_1(s9_1,6);
%-----------------------------------------------------------------------
% Raw data sorting for file 2
k_2=find(~isnan(data_2(:,1)));
leng_2 =length(k_2);
d0_2=k_2(1);
m_2=1;
a1_2=1;
```

```
while k_2(m_2)==d0_2
    s0_2(a1_2)=k_2(m_2);
    m_2=m_2+1;
    d0_2=d0_2+1;
    a1_2=a1_2+1;
end
 d1_2=k_2(m_2);
a2_2=1;
while k_2(m_2)==d1_2
    s1_2(a2_2)=k_2(m_2);
    m_2=m_2+1;
    d1_2=d1_2+1;
    a2_2=a2_2+1;
end
 d2_2=k_2(m_2);
a3_2=1;
 while k_2(m_2)==d2_2
    s2_2(a3_2)=k_2(m_2);
    m_2=m_2+1;
    d2_2=d2_2+1;
    a3_2=a3_2+1;
end
 d3_2=k_2(m_2);
```

```
a4_2=1;
while k_2(m_2)==d3_2
    s3_2(a4_2)=k_2(m_2);
    m_2=m_2+1;
    d3_2=d3_2+1;
    a4_2=a4_2+1;
end
 d4_2=k_2(m_2);
a5_2=1;
while k_2(m_2)==d4_2
    s4_2(a5_2)=k_2(m_2);
    m_2=m_2+1;
    d4_2=d4_2+1;
    a5_2=a5_2+1;
end
 d5_2=k_2(m_2);
a6_2=1;
while k_2(m_2)==d5_2
    s5_2(a6_2)=k_2(m_2);
    m_2=m_2+1;
    d5_2=d5_2+1;
    a6_2=a6_2+1;
end
```

```
 d6_2=k_2(m_2);
a7_2=1;
while k_2(m_2)==d6_2
    s6_2(a7_2)=k_2(m_2);
    m_2=m_2+1;
    d6_2=d6_2+1;
    a7_2=a7_2+1;
end
 d7_2=k_2(m_2);
a8_2=1;
while k_2(m_2)==d7_2
    s7_2(a8_2)=k_2(m_2);
    m_2=m_2+1;
    d7_2=d7_2+1;
    a8_2=a8_2+1;
end
 d8_2=k_2(m_2);
a9_2=1;
while k_2(m_2)==d8_2
    s8_2(a9_2)=k_2(m_2);
    m_2=m_2+1;
    d8_2=d8_2+1;
    a9_2=a9_2+1;
```

```
end
 d9_2=k_2(m_2);
a10_2=1;
while k_2(m_2)==d9_2
    s9_2(a10_2)=k_2(m_2);
    m_2=m_2+1;
    d9_2=d9_2+1;
    a10_2=a10_2+1;
end
 d10_2=k_2(m_2);
a11_2=1;
while k_2(m_2)==d10_2
    s10_2(a11_2)=k_2(m_2);
    m_2=m_2+1;
    d10_2=d10_2+1;
    a11_2=a11_2+1;
end
 d11_2=k_2(m_2);
a12_2=1;
while k_2(m_2)==d11_2
    s11_2(a12_2)=k_2(m_2);
    if m_2~=leng_2
    m_2=m_2+1;
```

```
    end
    d11_2=d11_2+1;
    a12_2=a12_2+1;
end



%-------------------------TIME DOMAIN ANALYSIS ------------------
% Raw Data Plot

% Time-force plot
 figure (1)
% time plot for file 1
subplot (3,3,1)
plot(time1_1,touch1_1)
subplot (3,3,2)
plot(time1_2,touch1_2)
subplot (3,3,3)
plot(time1_3,touch1_3)

% time plot for file 2
subplot (3,3,4)
plot(time2_1,touch2_1)
```

```
subplot (3,3,5)
plot(time2_2,touch2_2)
subplot (3,3,6)
plot(time2_3,touch2_3)

% time plot for file 3
subplot (3,3,7)
plot(time3_1,touch3_1)
subplot (3,3,8)
plot(time3_2,touch3_2)

%----------------------FAST FOURIER TRANSFORM-------------------------
function [ f1,f2,f3,Pyy1,Pyy2,Pyy3] = data_fft(time1,time2, time3, touch1, touch2, touch3)
point1=length(time1);
sr1=length(time1)/max(time1);
f1=fft(touch1,point1);
Pyy1 =f1.*conj(f1)/point1;
f1=sr1*(0:point1/2)/point1;
Pyy1(1)=0;
Pyy1 = Pyy1(1:point1/2+1);
 point2=length(time2);
sr2=length(time1)/max(time1);
f2=fft(touch2,point2);
```

```
Pyy2 =f2.*conj(f2)/point2;

f2=sr2*(0:point2/2)/point2;

Pyy2(1)=0;

Pyy2 = Pyy2(1:point2/2+1);

point3=length(time3);

sr3=length(time3)/max(time3);

f3=fft(touch3,point3);

Pyy3 =f3.*conj(f3)/point3;

f3=sr3*(0:point3/2)/point3;

Pyy3(1)=0;

Pyy3 = Pyy3(1:point3/2+1);


end


%****New matlab code for real fft (Modified and adopted with permission from the Human Performance Lab, University of Calgary)


function [out] = fft_real_vvt(x,inv)

%see fft_test.m for more information

%fft_real_vvt returns the fourier transform of the signal on a set of

%normalized axes; The length of the signal should be a power of 2.

%out is forward FFT if inv = 0; the imag part is the projection onto the

%-sin(2pi * f) axes. thus the -imag is the actual fourier coeficient.
```

```
%out is the inverse fft if inv = 1;
%out is the powerspectrum if inv = 2;
%T = N*dt;
%df = 1/T;
%frequency = (k-1) * df; with k = (1:Nyquist_frequency_ind);
%Nyquist_frequency = Nyquist_frequency_ind * df
% power is: pfx = fx .* conj(fx); %power is independent of dt. Power has unities of x squared.
%sum(pfx) = sum(x.*x) or sum(pfx) * dt = sum(x.*x) *dt is energy. dt = T/N
%pfx/df is power spectral density. This makes the amplitude of the spectrum
%independent of T or in turn of 0 padding.
%the first value of fft_real_vvt(x) / sqrt(N) is mean(x).



if inv == 0 || inv == 2 %do forward fourier transform
   si = size(x);
   if si(1) < si(2) %then we have a row vector and chang it to a column
      x = x';
   end
   N = size(x,1);
   Nyquist_frequency_ind = N/2 + 1;
   k = (1:Nyquist_frequency_ind);
   normalization_operator = zeros(Nyquist_frequency_ind,1) + sqrt(2/N);
   normalization_operator(1) = 1/sqrt(N);
```

```
    normalization_operator(end) = 1/sqrt(N);
    fx = fft(x);
    out = fx(1:Nyquist_frequency_ind) .* normalization_operator; % this is real_fft of vincent
    if inv == 2
       out = out .* conj(out);%this is = pfx, power spectrum
    end

else %do inverse fourier transform
    si = size(x);
    if si(1) < si(2) %then we have a row vector
       x = x';
    end
    Nyquist_frequency_ind = size(x,1);
    N = (Nyquist_frequency_ind -1) * 2;
    normalization_operator = zeros(Nyquist_frequency_ind,1) + sqrt(2/N);
    normalization_operator(1) = 1/sqrt(N);normalization_operator(end) = 1/sqrt(N);
    x = x ./ normalization_operator;
    x2 = flipud(x(2:Nyquist_frequency_ind -1));
    x = [x;conj(x2)];
    %a multiplication with a complec number e.g. when computing a time shift
    %causes the degenerated fourier coeficients to become complex.
    %They have to be set to real.
    x(1) = real(x(1)); x(Nyquist_frequency_ind) = real(x(Nyquist_frequency_ind));
```

```
    out = ifft(x);
end

%------------------WAVELET BASED FILTERING-------------------------------------

function [sig_filtered, f] = WaveletFilter14( signal, dt, cf, mode, type,test )
% H_WAVELETFILTER Written by vvt Oct 20th, 2006.
%   Computes the wavelet coefficients of:
%       wvlt = (f/cf)^mode * exp( (-f/cf+1) * mode )
%
%   type indicates if high or low pass the cases are:
%       1: low pass retain 100% of what is below cf.
%       2: low pass remove everything above cf.
%       3: high pass retain 100 % of what is above cf.
%       4: high pass remove everything that is below cf.
%       5: band pass what is defined by the wavelet.
%
% vvt: this has to be adapted for long signals by chopping the signals.

transposed = 0;
% make sure we have a columnvector
if size(signal,2) == 1
    signal = signal';
```

```
    transposed = 1;
end

%Determine length of signal
[rows input_length] = size(signal);

%adjust signal to be as close to 0 at the ends. readjust at the end. Do
%this by subtracting the average bias from the entire signal.
bias = (signal(:,1) + signal(:,end))/2;
signal = signal - repmat(bias,1,input_length);

%Determine next power of 2 and expand the matrix, and df.
%ceil - round the elements of x to the nearest integers towards infinity.
%x=b^y is the same as y=logb(x); singal length = 2^x, x=log2(signal length)
%loga(x)/loga(b)=logb(x) so to find what power of 2 is closest to the
%length of the signal, you do the following:
input_length_expanded = 2^ceil(log(input_length)/log(2));
T = input_length_expanded * dt;
df = 1/T;
signal(rows,input_length_expanded) = 0;

% index of Nyquist frequency
IND_NYQ = input_length_expanded/2;
```

```
frequency_index = 1:IND_NYQ+1;
%remember (index -1)*df = frequency if index starts at 1.
index_of_cf = floor(cf/df + 1);
f_cf = (frequency_index - 1) * (df/cf);
f_cf = f_cf(2:end);

% find wavelet coefficients as a function of the frequency
wvlt = exp( ( -f_cf + 1 +log(f_cf)) * mode );
wvlt = [0 wvlt]; %because log(0) is not possible.
wvlt_neg = 1 - wvlt;

switch type
   case 1
      filter = [ones(1,index_of_cf) wvlt(index_of_cf+1:IND_NYQ+1)];
   case 2
      filter = [wvlt_neg(1:index_of_cf) zeros(1,IND_NYQ+1 - index_of_cf)];
   case 3
      filter = [wvlt(1:index_of_cf) ones(1,IND_NYQ+1 - index_of_cf)];
   case 4
      filter = [zeros(1,index_of_cf)  wvlt_neg(index_of_cf+1:IND_NYQ+1)];
   otherwise
      filter = wvlt;
end
```

```
f.values = filter; f.frequency_range = (frequency_index - 1) * df;

filter = [filter  fliplr(filter(2:IND_NYQ))];

fsig = fft(signal, [], 2);


if test

    pfsig = fsig(1:IND_NYQ).*conj(fsig(1:IND_NYQ));

    pfsig(1) = 0;
```

Appendix C- Copyright Permission

Permission request

Request to reproduce figures or tables in other publications or journals: There is no need to obtain permission if copyrights of the figures or tables belong to Ivyspring International Publisher. Please acknowledge the original source of publication in our journal with full citation. If the copyrights of the figures or tables belong to other publishers or authors, please contact the original publishers or authors for permissions.

Authors or co-authors: As an author or co-author of the article, you are free to include or reuse any part of the materials in your thesis or other publications that you write, with citation of the original source in our journal. There is no need to obtain permission.

Terms of use

By accessing this web site, downloading, printing, or reading any article published in Theranostics (Journal), you are stating that you agree to all of the following terms and conditions:

• In no event shall the Journal, its publisher, editors or anyone involved in the Journal be liable to you or any other party on any legal theory, for any special, incidental, consequential, punitive, exemplary or any damages whatsoever arising out of or in connection with the use of any material in this web site or material published in the Journal, whether or not advised of the possibility of damage.

• The content of this web site and the materials published in the Journal are provided "as is" without warranty of any kind, either expressed or implied, including, but not limited to, the implied warranties of merchantability, fitness for a particular purpose, non-infringement, accuracy, completeness, or absence of errors.

• Statements or methods presented in the articles are those of the authors and do not constitute an endorsement by the editors or the publisher. The information contained in the articles must not be used as medical or any other advice. Nothing in the Journal or on this web site shall be deemed to be a recommendation of, endorsement of, or a representation as to a third party's qualifications, services, products, offerings, or any other information or claim.

• You agree to indemnify and hold the Journal and its editors, publisher, and authors harmless from any claim or demand, including legal and accounting fees, made by you or any third party due to or arising out of your use of this web site, your access, reading or transmitting of the Journal articles, or your violation of these Terms of Use.

• The Journal reserves the right, at its sole discretion, to change the terms and conditions of this agreement at any time without notice and your access of this web site will be deemed to be your acceptance of and agreement to any changed terms and conditions.

Privacy

Visitors' information such as IP addresses, referring site, date/time, etc. might be collected. This information and other personal information sent through forms in this web site is used for the Publisher's purpose only.